Technical University of Denmark

Jordi Martínez Díaz

A Comparison of Nonlinear Media for All-Optical Signal Processing

Master's Thesis, April 2013
Copenhagen, Denmark

DTU Fotonik
Department of Photonics Engineering

JORDI MARTÍNEZ DÍAZ

A Comparison of Nonlinear Media for All-Optical Signal Processing

Master's Thesis, April 2013

Supervisors:
Christophe Peucheret, Professor at the Photonics Engineering Department of DTU
Ivo Montrosset, Professor at the Department of Electronics of Politecnico di Torino

DTU - Technical University of Denmark, Kgs. Lyngby - 2013

A Comparison of Nonlinear Media for All-Optical Signal Processing

This report was prepared by:
Jordi Martínez Díaz

Advisors:
Christophe Peucheret, Professor at the Photonics Engineering Department of DTU
Evarist Palushani, Postdoc at the Photonics Engineering Department of DTU
Dragana Vukovic, Ph.D student at the Photonics Engineering Department of DTU
Ivo Montrosset, Professor at the Department of Electronics of Politecnico di Torino

DTU Fotonik Department
High-Speed Optical Communications
Technical University of Denmark
Ørsteds Plads, Building 343
2800 Kgs. Lyngby
Denmark
Tel: +45 4525 6352

Project period:	October 2012 - April 2013
ECTS:	30
Education:	MSc
Field:	Telecommunications Engineering

Abstract

This thesis is focused on benchmarking different nonlinear media that are currently used for all-optical signal processing. The materials survey has been based on both low linear losses and highly nonlinear characteristics. We firstly introduce a general knowledge about nonlinearities in the optical communications field before leading the reader to the analysis of such nonlinear materials properties. Some analytical indicators found in the literature review allow for getting a first rough comparison. Nonetheless, the different detrimental effects that we describe hereinafter such as Stimulated Brillouin Scattering, Two Photon Absorption and Free Carrier Absorption require numerical models in the analysis. Three numerical methods are employed in order to estimate more accurately the Conversion Efficiency considering the losses resulting from such phenomena in the wavelength (frequency) conversion process. Finally, a power-minimisation along with a length-optimisation provide us with a global comparison embracing some promising nonlinear materials. Such a benchmark shows when positive Conversion Efficiency (i.e. parametric gain) can be achieved by the elected media.

Acknowledgements

First of all, I would like to thank all the people who made this possible, to the ones who accompanied me during my stay abroad making it an unforgettable experience. It really helped me on carrying out this thesis. Secondly, I really need to dedicate my work to all my colleagues that have supported me throughout my degree in Barcelona at the UPC technical school.

Secondly, I want to show gratitude to all my advisers in the DTU, Christophe Peucheret, Evarist Palushani, Dragana Vukovic and Francesco Da Ros for their tireless assistance during the whole Thesis period. I cannot be more grateful for all the knowledge they provided me with in addition to the good work environment. Besides, I want to thank Professors Ivo Montrosset (Polito) and J. Maria Gene (UPC) to make my Master Thesis possible.

Finally, and more important, this project has been feasible thanks to the endless back-up from my parents and my family. Without their support during all my academic and life experiences, especially in the last two years, it would have been more difficult to make it.

To all of them, thank you very much.

Table of Contents

List of Figures

List of Tables

Nomenclature

CE	Conversion Efficiency
CW	Continuous Wave
DFG	Difference Frequency Generation
DFWM	Degenerate Four Wave Mixing
DSF	Dispersion Shifted Fibre
FCA	Free Carriers Absorption
FOM	Figure Of Merit
FWHM	Full Width at Half Maximum
FWM	Four Wave Mixing
HNLF	High Nonlinear Fibre
NLO	Nonlinear Optics
NLSE	Nonlinear Schrödinger Equations
OPA	Optical Parametric Amplifier
SBS	Stimulated Brillouin Scattering
SBST	Stimulated Brillouin Scattering Threshold
SFG	Sum Frequency Generation
SHG	Second Harmonic Generation
SPM	Self Phase Modulation
TPA	Two Photon Absorption
XPM	Cross Phase Modulation

CHAPTER 1

Introduction

The use of optical communications all over the world keeps continually increasing due to their good performance under high-speed conditions. It all started, as in most of the cases, within short-range communication links, however, it has already been and will continue being changed into long-haul systems. Therefore, some solutions had to be thought in order to keep the information well preserved all along the link. All required components have the same importance into the design ambit, from the emitting source (the laser), going through the fibre spans and ending onto the receiver.

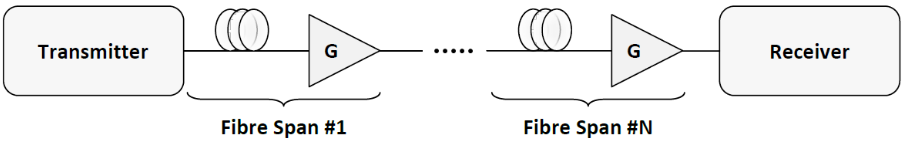

Figure 1.1: Scheme of an optical communications link. Both transmitter and receiver have been represented together with different fibre spans (long haul), each one consisting of a fibre link and an amplifier box.

Looking at the fibre span part, one can appreciate both, the light conduction path (fibre) and the amplifying block. Even though newly used fibres present really low losses (e.g. $\sim 0.2\, dB \cdot km^{-1}$), after long distances the transmitted signal suffers from this attenuation bringing it, then, down to levels where information misinterpretation could occur. Here comes the amplifier, which has the goal of signal amplification. Throughout many years such amplification has been made in the electrical domain using the so-called optoelectronic devices, which are the optical-to-electrical (OE) and the electrical-to-optical (EO) transducers. The exchange between these domains has been needed owing to the lack of resources in the optics, nevertheless great advances has already been demonstrated. Hence, this necessity of using electrical signal processing can be spared laying all the responsibility on optical amplifiers. Mostly, the so-called EDFAs (Erbium Doped Fibre Amplifiers) have lately been used for such objective. Yet, it is pursued the use of nonlinear media in order to get better performances. High-Nonlinear Fibres (HNLFs) will be presented since they provide high amplification. On the other hand, waveguide structures will be analysed since they allow for integrated circuits, which is one of the nowadays sought goals. Concretely, the main goal for this work consists in compare different nonlinear media intended for such amplification part.

Finding out which is the most appropriate media for your design can be a rough task. So, part of this process has been presented hereafter. One either hears from somebody or reads in somewhere that some of the groups have been working with such material, but is it the one that meets your requirements? It is known that various studies have been performed using the same materials and they differ in the results which is totally normal, considering the fact that is almost impossible to get twice the same exact design. Besides, not all the studies are carried under the same conditions, their goals might be slightly different. In this work what has been done is to benchmark from different sources so as to facilitate the decision process, saving the reader from all the research. It is worth mentioning that the state-of-the-art examples have always been chosen, though sometimes was not possible to find such information. It is not an easy job to gather all the information needed for this kind of comparison, since some of the properties are from time to time eluded.

The comparison will be made by means of Four-Wave Mixing (FWM) (hereafter described) which is a nonlinear effect resulting from the interaction of different signals. Hence, the list of materials under consideration has been made taking only the nonlinear ones allowing for what is known as nonlinear optics (NLO) processes. Thus, these so-called optical parametric amplifiers (OPA) can be fabricated in different both material and structure. The former can be (among others) either pure or doped Silica High-Nonlinear Fibres (HNLF); Silicon compounds such as crystalline (c-Si), amorphous (a-Si) or nitride (Si_xN_y); Chalcogenide glasses, for instance arsenic-sulphur (As_2S_3), arsenic-selenium (As_2Se_3) or germanium-arsenic-selenium ($Ge_{1-x-y}As_xSe_y$); and lately some groups are investigating in the III-V group of materials such as aluminium-gallium-arsenic ($Al_{1-x-y}Ga_xAs_y$), indium-phosphide (InP) or indium-gallium-phosphide (InGaP). Here it will be presented both fibres and waveguides structures.

Nonetheless, working with nonlinear media entails some effects that can become either useful or detrimental in our system. They have to be separated into two main groups, which are the second-order and the third-order nonlinearities ($\chi^{(2)}$ and $\chi^{(3)}$, respectively). The former can be, for example, second harmonic generation (SHG), sum frequency generation (SFG) or difference frequency generation (DFG). The second group can be shown thanks to the Kerr effect (presented later on) as self-phase modulation (SPM), cross-phase modulation (XPM), four-wave mixing (FWM), Raman and Brillouin scattering, or two-photon absorption (TPA). In the present case, just the stimulated Brillouin scattering (SBS) and the TPA are considered as negative effects to our scheme although some of them are presented in the following chapter. The author remarks that much of the results reported in here are obtained under the FWM scenario since it is widely used for the parametric amplification as well as in other applications not belonging to the scope of this project. Specifically the degenerate four-wave mixing (DFWM) has been contemplated, always in the continuous-wave approach (CW) working at the telecommunications band (C-band), which implies $\lambda \sim 1550\,nm$ $(f \sim 193\,THz)$.

Last but not least, let us clarify how we get the comparison of all these media. From all the previous phenomena, the one considered in here is the degenerate four-wave mixing (DFWM) since it provides us with a scheme that facilitates the comparison in terms of amplification. More specifically, what comes into play here is the frequency (wavelength) conversion efficiency coefficient (CE), which gives us the amplification in the newly generated signal (idler) at the output with respect to the signal at the input. This is clearly stated in the next chapter.

This document is divided into 4 more chapters in addition to this introduction. Firstly, in Chapter 2 a general background knowledge about nonlinear optics is presented. The aforementioned nonlinear processes described by the respective susceptibilities $\chi^{(2)}$ and $\chi^{(3)}$ are described. Secondly, both the effects of TPA and SBS are more deeply exposed in Chapter 3 together with different analytical and numerical models used throughout the thesis in order to classify such nonlinear media. Thirdly, Chapter 4 is presenting the results obtained along the simulations. Moreover, a comparison between the different selected nonlinear media is displayed. Finally, the conclusions and some possible future work are given in the last Chapter 5.

CHAPTER 2

Theoretical Background

All-optical signal processing has lately been raising more and more interest in the scientific community, willing to avoid the electrical domain and thereby, reducing power consumption while increasing both bandwidth and capacity. One of the ongoing tasks is the utilisation of the optical parametric amplifiers (OPAs) instead of switching to the electrical domain through opto-electronic (OEO) transducers. Consequently, it leads us to nonlinear optics (NLO), in what parametric amplification is based. However, an open-ended research is still being carried out in order to decide which materials could meet the requirements in terms of either gain or conversion efficiency, together with all the nonlinear effects that could accompany to the implementation.
This chapter is settling the reader into the nonlinear optics by presenting some of the more relevant aspects (with relation to this study) emerging in this specific branch of the optical communications. Mostly, the theory has been extracted from [1–4]. As an introduction, the OPA's main concept is stated, followed by a general view of some of the nonlinear effects commented before. In the one hand, the $\chi^{(2)}$ nonlinearities such as second-harmonic generation and, sum- and difference-frequency generation. On the other hand, phenomena pertaining to $\chi^{(3)}$ nonlinearities including Kerr effects, self- and cross-phase modulation, and (degenerate) four-wave mixing are described. Notice that the latter is mainly used all over this thesis so as to get the desired benchmark by studying how it behaves on different materials.

2.1 Optical Parametric Amplifier

The promising advances in NLO lead us to be optimistic when it concerns to the all-optical schemes. In order to get the amplification in the optical regime one needs to benefit from the parametric nonlinear properties of some materials. The process is simply based on launching the signal into either the waveguide or the nonlinear fibre together with one or two pumps. As a consequence, an interaction between those input signals occurs bringing them at the output along with idler waves resulting from such interaction. Fig. 2.1 shows the scheme of an OPA.

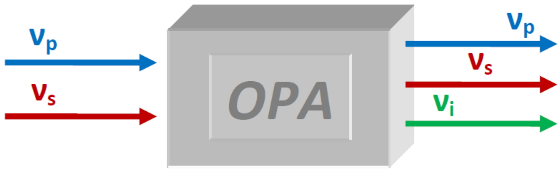

Figure 2.1: Scheme of an optical parametric amplifier. Only one pump power is launched with the signal.

Note that some approximations have been made in Fig. 2.1 since only 3 waves are interacting unlike some other usual cases where at least 4 waves are considered. Besides, not only one idler signal is produced at the output but lots of them, yet they have not been taken into account because of their negligible contribution to the analysis.
In the energy conversion from the pump to both the signal and the idler signals there is no such important heating effect on the material in comparison with that of the electrical case making them a good choice for high-power systems, but still, little thermal variations could become detrimental in some of the media when high powers are used. It is worth remarking that the law energy conservation is always fulfilled when the incident photons through the pump channel are separated giving rise to two other signals. Note that OPAs just amplify whilst being pumped, no storage elements are included in such devices. Moreover, these output idlers can be tuned at the desired wavelength so that one can work in another range for the due application (namely optical parametric generation). This wavelength conversion effect has more deeply been presented in the following four-wave mixing section as well as the phase matching condition, determining in these parametric amplifiers, since allowing for degeneracy in the frequency conversion between the interacting waves makes the amplifier be phase-sensitive.

Although in some cases pulsed signals are used owing to their extremely high peak powers, hereafter the continuous wave (CW) assumption will be considered. Additionally, $\chi^{(3)}$ nonlinearities have been considered in the development of this project albeit in so many other examples $\chi^{(2)}$ nonlinearities are investigated in the ambit of parametric amplification. While the scope of this thesis has not included exclusive attention to dispersion effects, they are the responsible for the enhancing/deterioration of gain bandwidth.

2.2 Nonlinear Optics

Given that we are working in this world of parametric processes we are in need of presenting a bit of nonlinear effects appearing on them. It is frequently attributed the commencement of nonlinear optics to initial discoveries at the early 60s when second-harmonic generation (SHG) was firstly observed thanks to the previous laser demonstration. This sort of sources permits the user to work at extremely high intensities which makes the nonlinear media exhibit their properties, inducing some changes to the waves travelling through them. As the name indicates, NLO stands for the branch of physics where the response to an optical field depends nonlinearly on the strength of the latter. Equivalently, nonlinearities become defined by the polarization ($\mathbf{P}$) when varying in a nonlinear manner with the applied optical field ($\mathbf{E}$). Hence, at working power ranges high enough (usually fulfilled by lasers) it can be described as [2]

$$\mathbf{P}(t) = \epsilon_0 \sum_{i=1}^{\infty} \chi^{(i)} \mathbf{E}^i(t) = \mathbf{P_L} + \mathbf{P_{NL}}, \tag{2.1}$$

where $\epsilon_0 = 8.854 \cdot 10^{-12} F/m$ is the vacuum permittivity, $\chi^{(i)}$ are the linear ($i = 1$) and nonlinear ($i > 1$) optical susceptibilities giving rise to the respective linear, $\mathbf{P_L}$, and nonlinear, $\mathbf{P_{NL}}$, polarizations. In turn, $\mathbf{E}$ denotes the optical field.

From the Eq. (2.1) one can see that infinite nonlinear interactions theoretically are participating, though contributions from susceptibilities higher than $\chi^{(3)}$ will be neglected from now on.

In order to present the behaviour of the light waves advancing through the nonlinear media, the wave-equation must be stated taking some approximations in the Maxwell equations (see Appendix) as the absence of both free charges ($\rho = 0$) and currents ($\mathbf{J} = 0$) since we are working with dielectric media, together with the nonmagnetic material assumption $\mathbf{B} = \mu_0 \mathbf{H}$ leading finally to the wave-equation [1]

$$\bigtriangledown^2 \mathbf{E} - \frac{1}{c^2}\frac{\delta^2 \mathbf{E}}{\delta t^2} = \mu_0 \frac{\delta^2 \mathbf{P_L}}{\delta t^2} + \mu_0 \frac{\delta^2 \mathbf{P_{NL}}}{\delta t^2}, \tag{2.2}$$

where $c = 299,792,458\ m/s$ and $\mu_0 = 4\pi \cdot 10^{-7}\ V \cdot s/(A \cdot m)$ are the speed of light and the permeability in the vacuum, respectively. It can be observed that polarization effects include both linear and nonlinear contributions, $\mathbf{P} = \mathbf{P_L} + \mathbf{P_{NL}}$. In the left-hand side of Eq. 2.2, the optical field interacting in the system is given by

$$\mathbf{E}(z,t) = \sum_{j}^{n} E_j(z) e^{-i\omega_j t} + c.c., \qquad E_j(z) = A_j(z) e^{ik_j z}, \tag{2.3}$$

where z and t stand for the propagation length and time, respectively, n define the number of interacting waves and $c.c.$ stands for the complex conjugate. $A_j(z)$ denotes the field amplitude while $k_j = \frac{n_j \omega_j}{c}$ represents the propagation constant, where the refractive index, n_j, is frequency-dependent.

Focusing on the nonlinearities, it is worth mentioning that second-order ones related to $\chi^{(2)}$ can occur only on those materials lacking inversion symmetry (namely noncentrosymmetric media) like some crystals. On the contrary, the so-called centrosymmetric materials (included some crystals as well) manifest the before-mentioned inversion symmetry making $\chi^{(2)}$ fade away. Accordingly, $\chi^{(3)}$ can emerge on either previous media. Hereinafter some of these peculiarities have briefly been detailed.

2.2.1 Second-Order Nonlinearities, $\chi^{(2)}$

Some crystals, when interacting with the light waves passing through them at high intensities, induce some effects on such waves. In addition to the target gain (or conversion efficiency, when idler signal is of interest) some effects come out of this light-matter interplay. In the present case, the following second-order nonlinearities have been depicted: second-harmonic generation (SHG), sum-frequency generation (SFG) and difference-frequency generation (DFG).

Second-Harmonic Generation

In some applications people often need to work at either the visible spectrum or the ultraviolet range of frequencies. In one case or the other, this shorter-wavelength conversion can be achieved by means of SHG. Besides, in Biology, where optical microscopy is needed or in surface diagnostics, SHG has likewise been used [4]. As mentioned before, this process is commonly considered as the starting point for the nonlinear optics.

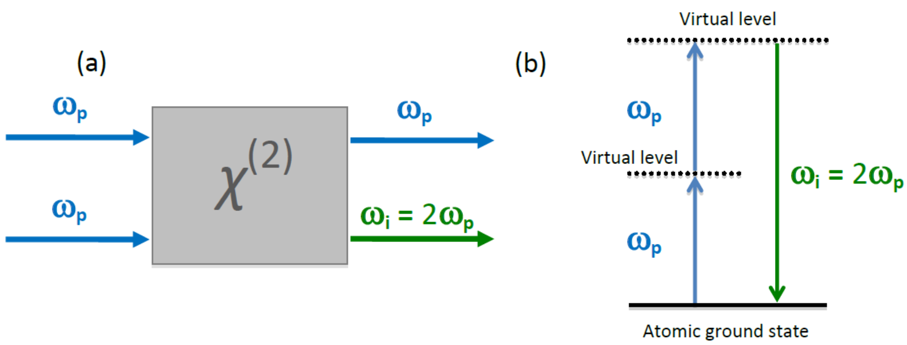

Figure 2.2: (a) Scheme of the second harmonic generation process through a nonlinear crystal (b) and its energy-level transitions diagram.

Fig. 2.2 visually describes the effect of this frequency doubling (also referred to as SHG), where the pumped signal at the input, ω_p, generates, usually towards the same direction, another signal at double-frequency (i.e. half the wavelength), $\omega_i = 2\omega_p$.
The incident electric field related to the laser beam is defined by $n = 1$ in Eq. 2.3. Afterwards, from Eq. (2.1) it can be seen, when propagating along the noncentrosymmetric crystal, the polarization created in the latter is represented by

$$\begin{aligned}\mathbf{P}^{(2)}(t) &= \epsilon_0\chi^{(2)}\mathbf{E}^2(t) \\ &= 2\epsilon_0\chi^{(2)}E_pE_p^* + (\epsilon_0\chi^{(2)}E_p^2 e^{\overbrace{-2i\omega_p t}^{\text{SHG}}} + c.c.).\end{aligned} \tag{2.4}$$

From Eq. (2.4) it can be seen the generation of this doubled-frequency wave. This is a phase-sensitive process in need of phase matching to become efficient. The latter (phase matching) is explained in the following four-wave mixing (FWM) subsection. As a nonlinear process, the intensity of the new-generated signal, ω_i, increases with the square of the pump intensity $P_i \propto P_p^2$, obviously until pump depletion appears since $P_i \leq P_p$ holds throughout the process.

Sum- and Difference-Frequency Generation

The processes of sum- and difference-frequency generation are analogous to that of Fig. 2.2 when not one but two signals are launched into such noncentrosymmetric crystal. The first (SFG) is pretty similar to the frequency doubling effect mentioned above, but taking $n = 2$ in Eq. 2.3. Indeed, one particular case occasionally used is the so-called third-harmonic generation, which consists of doubling one of the two input frequencies with respect to the other, resulting in a tripled-frequency output wave, being sometimes more efficient than the process obtained by the $\chi^{(3)}$ nonlinearities. On the other hand, DFG is often related to parametric amplification since the lower-frequency signal is amplified by the process per se (see Fig. 2.3), so that energy conservation is fulfilled.

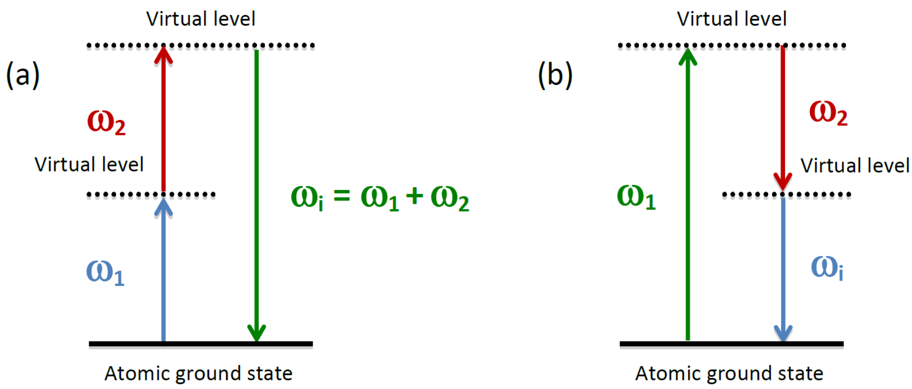

Figure 2.3: Energy-level diagram for (a) SFG and (b) DFG.

Fig. 2.3 shows both energy-level schematics for such processes.
From Eq. 2.1 the polarization field across the material has been derived to

$$\mathbf{P}^{(2)}(t) = 2\epsilon_0\chi^{(2)}[E_1E_1^* + E_2E_2^*] + \epsilon_0\chi^{(2)}(E_1^2e^{\overbrace{-2i\omega_1 t}^{\text{SHG}}} + E_2^2e^{\overbrace{-2i\omega_2 t}^{\text{SHG}}} + E_1E_2e^{\underbrace{-i(\omega_1+\omega_2)t}_{\text{SFG}}} + E_1E_2^*e^{\underbrace{-i(\omega_1-\omega_2)t}_{\text{DFG}}} + c.c.). \tag{2.5}$$

These phase-sensitive (phase matching condition modifies the conversion efficiency, CE) processes are usually employed for wavelength conversion to either ultraviolet and visible spectral range (SFG) or mid-infrared band (DFG).

2.2.2 Third-Order Nonlinearities, $\chi^{(3)}$

The third term ($\chi^{(3)}$) in Eq. 2.1 describes the polarization changes induced in the centrosymmetric materials (e.g. high-nonlinear fibres, HNLFs) due to third-order nonlinearities. Almost all media show such kind of properties. Let us have a look now at some of these high-intensity-caused effects owing to $\chi^{(3)}$ properties, for instance Kerr effect, four-wave mixing including the degenerate case (DFWM) and, finally, an introduction to the TPA and SBS effects.

Kerr Effect

Once the polarization is related to the electric field through $\chi^{(3)}$ susceptibility, one could say that the commonly named Kerr nonlinearities start occurring. Historically, it was firstly discovered by the physicist John Kerr in 1875, and it is defined by (and often referred to as) the intensity-dependent refractive index, by means of [2]

$$n = n_0 + n_2 I, \tag{2.6}$$

where n_0 and n_2 are the weak-field and the nonlinear refractive index, respectively, and $I = 2n_0\epsilon_0 c|E(\omega)|^2$ stands for the field intensity. Notice that n_2 is expressed in $\left[\frac{m^2}{W}\right]$.
This nonlinear (Kerr) refractive index leads to a wide variety of events that affect the travelling waves albeit only SPM and XPM are concisely commented below. The case when four waves are processed (three when degeneracy is supposed) has been described in the next subsection.
Whether the optical field stated in Eq. 2.3 (when $n = 1$) is crossing the device under high-intensity conditions, a phase-shift (Φ) is induced by the wave itself (self-phase modulation) which can be used, e.g., for spectral broadening and solitons creation. It is represented by

$$\Phi = (n_0 + n_2 I)\, k_0 L, \tag{2.7}$$

where $k_0 = \frac{2\pi}{\lambda}$, being λ the wavelength and L is the device length. Note that it has been considered the lossless fibres case. Nevertheless, losses could be included by utilising the effective length, $L_{eff} = \frac{1 - e^{-\alpha L}}{\alpha}$, instead of L.

On the other hand, when two waves are travelling along the medium and each wave is changing the other one's phase, then we have cross-phase modulation. Its usual applications consist of spectral broadening, lasers synchronisation or measuring tool. Neglecting other terms, the nonlinear shift can be described as

$$\Phi_{NL} = (I_1 + 2I_2)\, n_2 k_0 L, \tag{2.8}$$

where I_1 and I_2 are the intensities of both signals. One could see both the SPM and the XPM contributions to the phase shift, respectively. Notice that the factor 2 in the XPM term holds up as long as both beams are generated in the same polarization, otherwise it should be reduced by some factor [4].

Four-Wave Mixing

Many of the applications in the NLO field of research are based on the so-called FWM process. Main attention has been paid on it in this project since all the comparisons have been made under this scheme. Precisely, under the degenerate case, since only one pump has been taken into consideration.
The main difference between the previous effects and FWM is that the latter involve energy [5] exchange during the process. We are still looking into a phase-sensitive effect in need of phase matching in order to get high efficiency in the frequency conversion. Let us consider now $n = 3$ in Eq. 2.3. When the input signals (ω_{p_1}, ω_{p_2} and ω_s) are launched all together into the system, an extra signal is created in a symmetrical manner, thus meeting both the energy and the momentum conservation laws [3]

$$\sum_{j=1}^{2} \hbar\omega_{p_j} = \hbar\omega_s + \hbar\omega_i, \tag{2.9a}$$

$$\sum_{j=1}^{2} \hbar k_{p_j} = \hbar k_s + \hbar k_i, \tag{2.9b}$$

where ω_i and k_i stand for the newly generated idler signal frequency and propagation constant, respectively and $\hbar$ is the reduced Planck's constant. Eq. 2.9b is known as the phase matching condition, which is difficult to obtain in many occasions due to the dispersive behaviour of some of the materials. In case the system satisfies Eq. 2.9b the

maximum conversion efficiency (hence, the gain) is achieved.
Let us present the nonlinear coefficient

$$\gamma = \frac{n_2\omega}{cA_{eff}} = \frac{2\pi n_2}{\lambda A_{eff}}, \tag{2.10}$$

where n_2 is the nonlinear (Kerr) effective index and A_{eff} the effective area of the device (see Appendix). Note that frequency-dependence (ω_j) have been ignored, thus γ takes an average (constant) value for all the signals. After some approximations, such as single-mode propagation and neglecting pump depletion, and including the nonlinear effects governed by the above-defined γ, an effective phase-mismatch can be stated as [2]

$$\kappa \approx \Delta k_M + \Delta k_{NL}, \qquad \Delta k_{NL} = \gamma\left(\sum_{j=1}^{2} P_{p_j}\right), \tag{2.11}$$

where Δk_M is the phase mismatch due to the material dispersion described in Eq. 2.9b where $k_j = \dfrac{n_j\omega_j}{c}$. For simplicity, when considering only one pump signal (see Fig. 2.4), i.e. degenerate-FWM ($P_{p_1} + P_{p_2} = P_p$), the phase mismatch is finally given by [2]

$$\kappa \approx \underbrace{\left(\beta_2\Omega_s^2 + \frac{\beta_4}{12}\Omega_s^4\right)}_{\Delta k_M} + \overbrace{2\gamma P_p}^{\Delta k_{NL}}, \tag{2.12}$$

where β_2 and β_4 represent the second- and fourth-order dispersion parameters, respectively and $\Omega_s = \omega_p - \omega_s$ stands for the signal detuning from the pump frequency.
In practice, β_4 is often neglected. Moreover, instead of the group velocity dispersion (GVD) parameter β_2, sometimes the dispersion parameter D is utilized which can be written as

$$D = -\frac{2\pi c}{\lambda^2}\beta_2 = -\frac{\lambda}{c}\frac{d^2n}{d\lambda^2}. \tag{2.13}$$

Note that getting phase matching would imply an almost suppression of dispersion effects, which consists in working close to zero-dispersion wavelength, $\lambda = \lambda_{ZD}$, in Eq. 2.13. However, it is often considered the zero-dispersion condition as the phase-matching fulfilment by neglecting the nonlinear contribution ($2\gamma P_p$).

Two possible schemes, as shown in Fig. 2.4 could be used: two different pump signals, ω_{p_1} and ω_{p_2}, on the one hand, or just one pump signal providing two photons at the same frequency, $2\omega_p$, on the other.
In Fig. 2.4 both non-degenerate and degenerate FWM phenomena have been presented. Moreover, the energy conversion, i.e. the photons given by the pumps to both idler and signal waves, has been depicted (grey dotted line). The dotted lines illustrate both the signal (red) and the idler (green) at the output. The correlated gain (G) and conversion

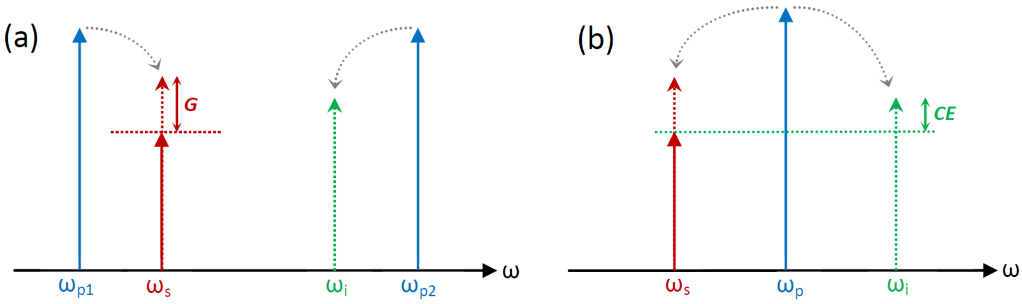

Figure 2.4: Schematic diagram for the (a) FWM and the (b) DFWM processes.

efficiency (CE) parameters have also been represented by showing the increase in power at the output after exchanging photons.

As already mentioned, in order to efficiently convert the input frequency by FWM process, the phase-matching requirement must be satisfied ($\kappa = 0$). Hence, the amplification to the output signals, ω_s and ω_i, becomes maximum. In accordance with Fig. 2.4, such amplifications are defined as follows

$$G = \frac{P_s^{out}}{P_s^{in}}, \qquad CE = \frac{P_i^{out}}{P_s^{in}}, \tag{2.14}$$

where P_s^{in} and P_s^{out} denote the signal powers at the input and the output, respectively and P_i^{out} is the idler power at the output.
From time to time, for simplicity, in the literature one could find the relation for CE with the powers taken at the output. They are directly related by means of $G = 1 + CE$. Henceforth, the use of gain is no longer used since all the comparisons have been made in terms of conversion efficiency.

FWM has been used in different kind of applications, mainly focused on parametric processes such as supercontinuum generation (spectral broadening when pulsed lasers are used), phase conjugation or parametric amplification. Besides, it has been useful for spectroscopy, as well as holography and optical image processing [4]. Nevertheless, it can be detrimental in wavelength division multiplexing (WDM) systems causing cross-talk between channels. In the present work, much attention has been paid in the study of the idler signals behaviour, which brings us to analyse how the material properties affect to the conversion efficiency parameter.
Firstly, as a rough approximation, let us consider the following inputs influencing the performance of the CE

$$CE = f\left(\gamma,\ P_p,\ \alpha,\ \kappa\right), \tag{2.15}$$

where

- γ is representing the effect from nonlinearities over the idler wave generation. Certainly, it will strongly modify the newly generated power, thus, the conversion efficiency. The stronger the γ, the higher the CE. Therefore, laborious work has been focused on finding high-nonlinear materials.

- P_p is determinant since it will shape the nonlinear contributions to the system. Not to mention that the pump is the one transferring photons to the signals of interest. It is worth commenting that pump-depletion and gain saturation must be avoided in order to get better efficiency. In addition, extremely high powers can become harmful.

- α denotes the linear losses which might be one of the most limiting influence in the scheme. Even though they cannot be avoided in any way, much progress has been achieved in minimizing them. The most lossy schemes appear when using waveguides while fibres already present really low losses. The loss will determine the optimum length, L_{opt}, of our device.

- κ stands for the aforementioned phase mismatch. It is rather difficult to meet the phase-matching condition in some cases, shrinking then the maximum CE achievable. Dispersion effects, aside from varying κ and n, will also characterise (along with L) the gain-bandwidth.

The main goal is to obtain high-enough conversion efficiency ($CE \geq 1$) so that conventional amplifiers can be avoided, hence, no extra noise is added to the system. It has graphically been represented in Fig. 2.5, where the amplifier characterised by the gain factor, G, and the noise factor, NF, is adding noise, P_n, to the useful signal, P_i.

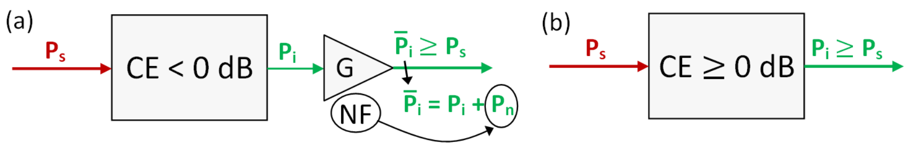

Figure 2.5: Schematic representation whether (a) noise is added or (b) not due to the conventional amplifier.

Different schemes from early work has been presented in Chapter 3 in order to study either analytically or numerically the conversion efficiency in the degenerate four-wave mixing process.

Two-Photon Absorption and Stimulated Brillouin Scattering

By contrast, the light-matter interaction also present non-parametric processes, where the quantum state of the material is no longer invariable. This means that, contrary to the previous effects, either energy-exchange exists between the waves and the centrosymmetric material (TPA) or the process become inelastic, generating backscattered light from the launched field due to molecular vibrations in the material (SBS).

In the early 30s M. Göppert-Mayer described the TPA effect for first time and it was demonstrated afterwards by W. Kaiser and C. G. B. Garrett in 1961 [6]. It affects the system with an extra-loss term since the material is absorbing two photons while travelling through it, producing a decrease in the transmitted power. The absorption process can be understood through Fig. 2.6.

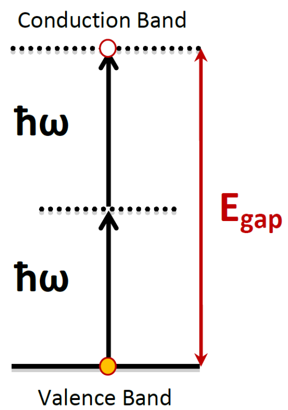

Figure 2.6: Energy-level diagram for TPA process.

From the scheme in Fig. 2.6 it can be seen the two photon jumping to the excited state through an energy leap of $\hbar\omega$ (each one). Hence, TPA can occur only in those media whose band-gap energy (E_{gap}) allow for such energy absorption, meaning that

$$E_{gap} \leq 2\hbar\omega. \tag{2.16}$$

Note that high intensities are still required, otherwise linear absorption (α) is more strongly affecting the system. Nonetheless, at important intensities TPA becomes considerable since its effect increases with the optical intensity, which is the same that saying the absorbed power is proportional to the square of the input power. In addition, TPA eventually induces the generation of free carriers in the system, limiting even more the performance. Even though TPA has been thought of as an adverse phenomenon in the present document, it has alternatively been related to a wide variety of applications like spectroscopy, lithography or power limiting amongst others [7].

On the other hand, L. Brillouin and L. Mandelstam in the 20s firstly discovered the scattering effects, which could also be understood as extra losses since energy from the pumped wave is transferred to a frequency-shifted and backscattered one (it can travel also forwards in the stimulated Raman scattering effect but it does not belong to the goal of this project), namely stimulated Brillouin Scattering (SBS).
In 1964, R. Y. Chiao et al. [8] initially tested the fact that when the intense field is launched into the device, thanks to the electrostriction phenomenon, the light interacts with the

acoustic waves of the material stimulating a backscattered, and so-called, Stokes signal at a down-shifted frequency not greater than [1, 2, 9–11]

$$v_B = \frac{2n v_A}{\lambda_p} \tag{2.17}$$

where v_A is the acoustic velocity of the material and the pump wavelength is (in here) chosen as $\lambda_p = 1.55\ \mu m$.

In order to analytically study the effect of SBS (see Chapter 3), the pumped signal has not been considered depleted, though, in practice, the higher the intensity of the pump (ω_p), the higher (nonlinearly increasing) the power of the Stokes wave (ω_S). That means, the former travelling wave becomes depleted at some point.

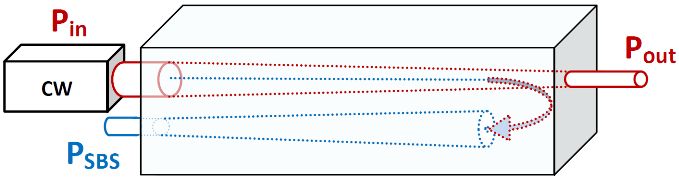

Figure 2.7: Theoretical scheme of the SBS effect in the material.

Fig. 2.7 presents the schematic for the backscattered wave due to the $\chi^{(3)}$ nonlinearities of the material. It is represented in red the pumped signal coming from the CW laser source, which travels along the device suffering from attenuation (dotted lines) while transferring power to the Stokes signal (in blue). One could appreciate that the latter is likewise weakened owing to the losses. Supplementary to this, it is worth recalling that the number of photons going backwards becomes increased provided the pump power keeps augmenting (see Fig. 2.8).

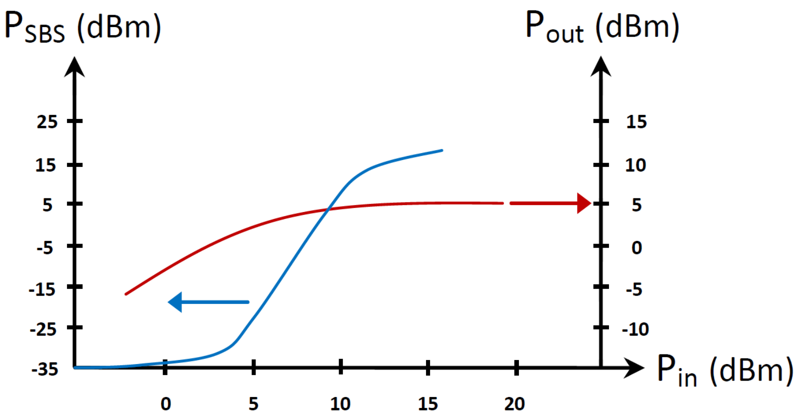

Figure 2.8: Example of the SBS behaviour in a 13 km-long Silica dispersion-shifted fibre (DSF).

The evolution of both signals has been represented in Fig. 2.8, taking as an example 13 km of a Silica dispersion-shifted fibre (DSF) [9]. Regarding the scheme in Fig. 2.7 the red curve shows the signal crossing the material in the forward direction while the blue one represents the backscattered power (P_{SBS}).

One of the principal differences between SBS and TPA is that the former is directly related to the configuration design (i.e. A_{eff}) while the latter is completely geometry-independent.

Analogously to the TPA, different applications have been connected to the SBS phenomenon [12] disregarding its negative contribution. Mainly, one can find nonlinear fibre amplifiers based on the SBS effect albeit fibre sensors, beam combiners or pulse delaying are benefiting from it as well. Thanks to the time delaying, SBS allows for slow-light generation [13–15], lately studied in order to enhance NLO's efficiency, although it has not been considered in this work.

CHAPTER 3

Modelling of Nonlinear Tools for the Comparison

Lately, the interest in nonlinear properties of some materials has noticeably been grown. From now on, the author has just considered the third-order nonlinearities in the comparison. As previously seen in Chapter 2, not all the consequences resulting from $\chi^{(3)}$ nonlinearities are positively affecting the performance. In order to carry out the main scope of this work, i.e. benchmarking different nonlinear media, some main parameters have been chosen, which are TPA and SBS as counter-propagating inputs from the one hand, and the CE as the comparison tool in itself, from the other.

3.1 Stimulated Brillouin Scattering Computation

Usually, most of the fibres present the mentioned acoustic characteristics reflecting the pumped light backwards, making the output (forward) wave seem saturated when high intensities are launched into the system. This is the consequence of the pump photon annihilation creating the new backscattered wave, which brings us to regard the conservation laws (Eq. 2.9), considering now the Stokes signal as an interacting wave. Accordingly, the Brillouin frequency shift is defined by the angle (θ) between pump (ω_p) and Stokes (ω_S) signals as (please, do not confuse the Stokes frequency, ω_S, with the signal one, ω_s) [1]

$$\Omega_B \approx 2\upsilon_A|\mathbf{k_p}|\sin\frac{\theta}{2}, \tag{3.1}$$

where $|\mathbf{k_p}| = \dfrac{2\pi n_p}{\lambda_p}$. The single-mode fibre approach has been considered, meaning that only two propagation directions in such fibre are possible, forwards and backwards. The former implies $\theta = 0$, hence no frequency shift exists, while the latter entails $\theta = \pi$, resulting in Eq. 2.17 whether $\upsilon_B = \frac{\Omega_B}{2\pi}$.

The signal travelling at that shifted-frequency, as previously mentioned, increases as the input intensity grows. It is governed by the so-called Brillouin gain, which describes the amplitude of such a signal. The variations in the medium's characteristics due to electrostriction phenomenon together with the chosen working conditions (λ_p) decide the maximum Brillouin gain. Different definitions could be found in the literature. Hereafter, two of them are presented, the first one defined in [1] and the second one in [10, 11] as

$$g_{Bmax} = \frac{8\pi^2\gamma_e^2}{n_p\lambda_p^2\rho_0 c\upsilon_A\Gamma_B}, \qquad g_{Bmax} = \frac{2\pi n_p^7 p_{12}^2}{c\lambda_p^2\rho_0\upsilon_A\Delta\upsilon_B}, \tag{3.2}$$

where γ_e and ρ_0 are the electrostrictive constant and the density of the media, respectively. The phonon (i.e. elastic vibrations) lifetime is defined as $T_B = \Gamma_B^{-1}$, usually taking values of the order of nanoseconds. On the other side, p_{12} is known as the elasto-optic coefficient, while $\Delta\upsilon_B = \frac{\Gamma_B}{2\pi}$ is the full-width at half-maximum (FWHM) of the Brillouin gain spectrum $g_B(\Omega)$, which normally takes the value of tens of MHz, reaching a higher order of magnitude when straining techniques are applied to the fibre [16].
Thereafter, $g_B(\Omega)$, which is considered to have a Lorentzian form, is given by

$$g_B(\Omega) = g_{Bmax}\frac{(\Gamma_B/2)^2}{(\Omega-\Omega_B)^2+(\Gamma_B/2)^2}. \tag{3.3}$$

It can be seen that the maximum g_{Bmax} is achieved at the Brillouin shift $\Omega = \Omega_B$. The latter consideration has been taken throughout the whole thesis when referring to g_B.
Eq. 3.3 has been defined under steady-state conditions which is acceptable only in a CW scheme and, considering the laser (Lorentzian) profile spectral width $\Delta\upsilon_p \ll \Delta\upsilon_B$. Otherwise, the before-mentioned maximum gain is diminished by a factor $1 + \frac{\Delta\upsilon_p}{\Delta\upsilon_B}$, increasing then, the threshold power defined below.

The next step is to analyse the effect that SBS induce to the field propagation as depicted in Fig. 2.7. Such an interaction between the pump and the Stokes waves has been described in here, considering firstly the CW scheme and secondly, the negligible differences between both frequency and the losses of the interacting waves, which means $\Omega_B \approx 0$ and $\alpha_p \approx \alpha_S \equiv \alpha$, respectively. Thirdly, the polarization of both signals has been thought of to be the same and invariable all over the device, particularly polarized along a main axis. Thus, the set of coupled equations that characterises the SBS turns out to be

$$\frac{dI_p}{dz} = -\left(g_B I_p I_S + \alpha I_p\right), \tag{3.4a}$$
$$-\frac{dI_S}{dz} = g_B I_p I_S - \alpha I_S, \tag{3.4b}$$

where $g_B = g_{B_{max}}$ is taken from Eq. 3.3 when $\Omega = \Omega_B$. Note that counter-propagation is considered when describing the Stokes field propagation in Eq. 3.4b. In addition, this general definition has not taken into account neither dispersion nor nonlinear effects unlike the Nonlinear Schrödinger Equations (NLSE) do [17]. Nonetheless, from now on the coupled equations have been taken under consideration in order to establish the SBS threshold, named as SBST.

Not only the above-named constrictions but the disregard of pump depletion has been as well contemplated. The first step then, consists in knowing the Stokes intensity waveform whether $I_p(z) = I_p(0)e^{-\alpha z}$ is considered to be the pump intensity interacting throughout the media. Hence, integrating Eq. 3.4b by using such I_p results in the counter-propagating wave by means of

$$I_S(0) = I_S(L)e^{g_B I_p(0) L_{eff} - \alpha L}. \tag{3.5}$$

Notice that the propagation direction is backwards as expected. The SBS contribution term is scaling with the effective length, L_{eff}. Given that the threshold is often sought in the power domain, the latter relation is alternatively expressed by considering $I_p(0) = \dfrac{P_p(0)}{A_{eff}}$.

Let us now move on to the threshold power computation. In the present section two different methods have been presented. The first one consists in analytically defining the threshold power whilst the second one is numerically simulating the system described by Eq. 3.4.

3.1.1 Stimulated Brillouin Threshold: Analytical Approximation

Generally, one procedure to calculate which is the maximum P_p allowed before its depletion becomes important, consists in the analytical computation. The starting point lies in the common definition stated as [10]

$$P_S(0) = \mu P_p(0), \tag{3.6}$$

which decides the amount of Stokes power at the input of the device by a fraction μ of the pump power. Regarding the latter parameter, different criteria have been settled when deciding which percentage of backscattered pump power should determine the threshold such as 100% $(\mu = 0, 1)$ in [1], 10% $(\mu = 0, 1)$ in [18] or 1% $(\mu = 0, 01)$ in [10, 17].
Later on, the more restrictive condition has been chosen, allowing solely 1% of the pump power as the Stokes power at $z = 0$.
The commonly used approximation of the SBST, directly related to the device properties,

becomes described as follows

$$P_{th} \approx \kappa \frac{A_{eff}}{g_B L_{eff}}, \tag{3.7}$$

where the constant κ, deeply demonstrated in [10], takes values usually within $[16, 21]$ depending on the adopted value of μ. It might be seen that $\kappa = 21$ is widely used in the related work.
Notice that P_{th} stands for $P_p(0)$ stated in the definition given by Eq. 3.6. Depending on the application field, such threshold may be desired either to be as low as possible so as to amplify the backscattered signal at low pump powers (i.e. Brillouin lasers) or high enough not to limit the intense power (by depleting it) required by efficient nonlinear effects (i.e. wavelength conversion).

Last but not least, in order to compare distinct media people often use the so-called Figure of Merit (FOM). Different ways to define the latter exist depending on the application [19], though in here a modification of the commonly used FOM (γL_{eff}) has been presented as [20]

$$FOM_{SBS} = \gamma L_{eff} P_{th}. \tag{3.8}$$

Combining eqs. (2.10), (3.7) and (3.8) the FOM is given by

$$FOM_{SBS} = \frac{2\pi\kappa n_2}{\lambda_p g_B}. \tag{3.9}$$

3.1.2 Stimulated Brillouin Threshold: Numerical Computation

On the other hand, in order to obtain a more precise conception about the SBS threshold, one needs to solve the set of coupled equations in Eq. 3.4 in a numerical manner, by using some computation software. Hereinafter, the Matlab® Tool has been utilised for the estimations.
Firstly, let us introduce the principal scheme under study somewhat modified in order to numerically picture the propagation behaviour. Therefore, knowing that the system defined in Eq. 3.4 merely accounts for stimulated influences, some adaptation has been performed in order to add the participation of spontaneous effects which, in turn, are somehow responsible for the SBS commencement [18, 21]. Such variations become specified as below

$$\frac{d\bar{P}_p}{d\zeta} = -\left(G_B\bar{P}_p\bar{P}_S + \alpha'\bar{P}_p + \beta_i'\bar{P}_p\right), \tag{3.10a}$$

$$-\frac{d\bar{P}_S}{d\zeta} = G_B\bar{P}_p\bar{P}_S - \alpha'\bar{P}_S + \beta_i'\bar{P}_p, \tag{3.10b}$$

where $\bar{P}_i = \frac{P_i}{P_p(0)}$, $\zeta = -\frac{z}{L}$, $G_B = \frac{g_B L P_p(0)}{A_{eff}}$, $\alpha' = \alpha L$ and $\beta_i' = \beta L$.

Note that normalisation of the respective parameters to L in space and to $P_p(0)$ in power have been made for computation simplicity. The last term β_i' stands for the spontaneous contribution somehow represented in Fig. 2.7 which is inducing the phenomenon start-up. The numerical computation model is based on a shooting algorithm, which gives rise to a solution for Eq. 3.10. It has graphically been depicted and afterwards, the step-by-step definition of the algorithm has been listed.

Secondly, an appropriate schematic for the proposal is given in the next Fig. 3.1. It has been represented the contour conditions taken for the later on described solution. Notice that for the present example a fibre has been depicted.

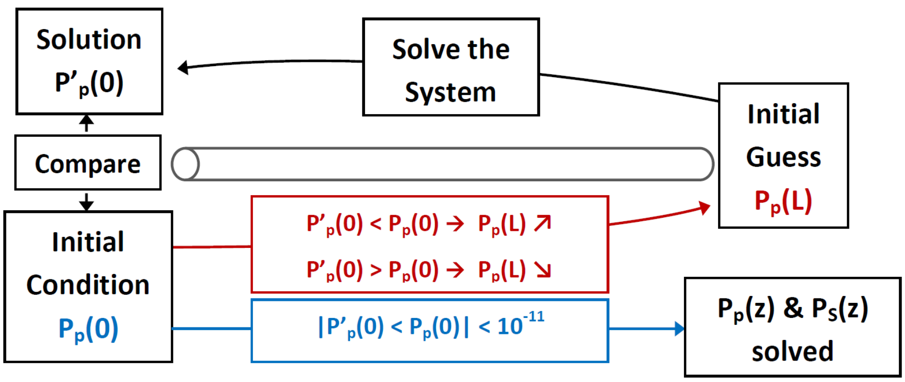

Figure 3.1: Graphical representation of the Shooting algorithm.

Concretely, the shooting algorithm can be readily interpreted by the following steps:

1. Guess a value for $P_p(L) = KP_p(0)e^{-\alpha L}$, where K is a percentage parameter.
2. Solve the coupled equations backwards obtaining a solution for $P_p'(0)$.
3. Compare such a solution to the initial condition decided for $P_p(0)$. The relation $|P_p'(0) - P_p(0)| < Tolerance$ must be fulfilled to consider the solution acceptable.
   a) if $P_p'(0) > P_p(0)$, the previous guess $P_p(L)$ is down-shifted. Consequently, the process is restarted from step 2.
   b) if $P_p'(0) < P_p(0)$, the previous guess $P_p(L)$ is up-shifted. Consequently, the process is restarted from step 2.

c) if $|P_p'(0) - P_p(0)| < 10^{-11}$, the system is considered solved, being 10^{-11} the chosen tolerance not to overrun Matlab® computation capacity.

4. Finally, $P_p(z)$ and $P_S(z)$ become described for the whole path.

It is worth mentioning that some other particularities have been considered in the algorithm in order to control the convergence speed in the guessing process together with the computation time. Nevertheless, this does not belong to the scope of this work.
Thirdly, once the algorithm has been clarified, the process can be completed stating the initial guess with $K = 0.5$.
The propagation of both the input pump and the Stokes waves along the fibre has been exemplified in Fig. 3.2. Notice that length axis has been normalized in the plot.

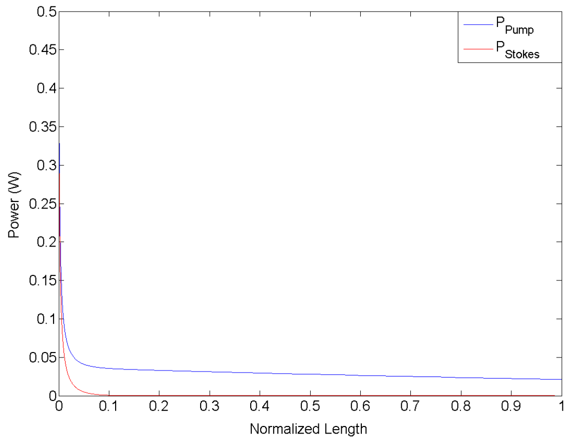

Figure 3.2: Both pump (blue) and Stokes (red) power propagations along the (normalized) fibre length.

The example depicted in Fig. 3.2 belongs to a Silica DSF characterised by $n_2 = 2.6 \cdot 10^{-20}\, m^2 \cdot W^{-1}$, $\gamma = 2.4\, W^{-1} \cdot km^{-1}$, $\alpha = 3 \cdot 10^{-4}\, dB \cdot m^{-1}$, $L = 8\, km$, $D = -1.6\, ps \cdot km^{-1} \cdot nm^{-1}$, $A_{eff} = 44\, \mu m^2$ and $g_B = 6.17\, m \cdot W^{-1}$ (see Table in Chapter 4). The working point has been thought of as $\lambda_p = 1.55\, \mu m$, $P_p(0) = 0.5\, W$, $P_S(L) = 0\, W$ and $\beta_i = 10^{-12}\, m^{-1}$.

3.2 Two-Photon Absorption Computation

As it has been seen so far, the marvellous properties of nonlinear media come accompanied by a few negative effects. In addition to such detrimental consequences, two-photon absorption appears frequently in some waveguides structures (occasionally in fibres) bringing the system performance down, too. Indeed, it is one of the effects that has importantly increased the interest in finding new nonlinear media, since some very promising materials (e.g. Silicon) are still limiting some applications due to their high TPA.

Considering that all-optical switching requires interactions with high powers and long lengths through materials with large n_2, TPA is often treated as a limitation to that [22–24].

Contrary to the SBS effect, whilst high intensity is still demanded, the phase matching is no longer a condition in TPA schemes [7]. Such power-condition has previously been presented in Eq. 2.16 and graphically depicted in Fig. 2.6.

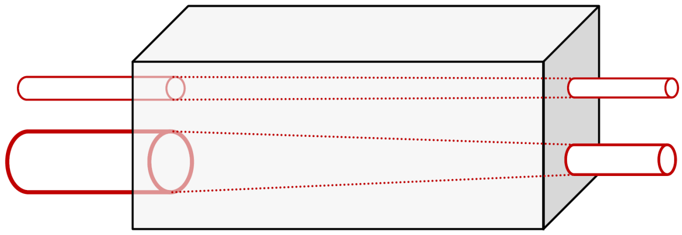

Figure 3.3: Graphical representation for the nonlinear reduction of the beam intensity owing to the TPA.

In Fig. 3.3 it has been pictured the nonlinear nature of such phenomenon, which behaviour meets the rule: the more power launched into the device (the lower beam in the scheme), the stronger the attenuation.
Different comparison paths has been found in the literature whether TPA is negatively contributing to the system. It is worth remarking that some applications are based on such effect albeit they are not exposed in this document. Regarding the comparison task, two main possibilities has been described. In the first place, one analytical process is provided, whereas a much more precise alternative, which is directly related to the CE parameter, will be described afterwards in Section 3.

Let us move on to the analytical interpretation of this geometry-independent nonlinear absorption and its consequence to the performance, such as power saturation. Despite a thorough study could be done, by means of molecular particularities describing the behaviour that we are looking into as seen in [25], the general definition for such beam propagating along the media has been described in here as

$$\frac{dI}{dz} = -\alpha I - \beta_{TPA} I^2, \tag{3.11}$$

where both linear and nonlinear absorption contributions have been taken into account. While α stands for the linear losses coefficient in $\left[\frac{1}{m}\right]$, β_{TPA} represents the so-called two-photon absorption coefficient measured in $\left[\frac{m}{W}\right]$.

Analogous to the SBS study, the two different comparison methods presented in the present work to compute the TPA phenomenon have not been acquired from the NLSE as in [26] but resulting from Eq. 3.11 on the one hand, and from a set of coupled equations on the other.
Hence, the analytical comparison taken into consideration is given by [7, 22]

$$P(L) = P(0)\frac{e^{-\alpha L}}{1 + \beta_{TPA} L_{eff} \frac{P(0)}{A_{eff}}}, \tag{3.12}$$

where no coupling losses have been included. It is worth mentioning that such a relation is considering peak powers, meaning that really high values can be used. It provides the behaviour of the power propagation whether both linear and nonlinear absorption are participating.

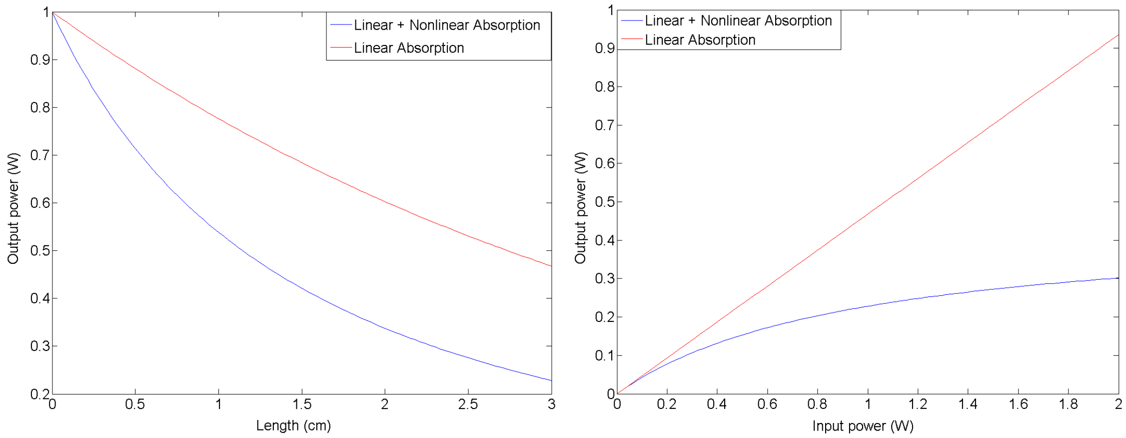

(a) Output power vs. length ($P_{in} = 1\ W$).

(b) Output power vs. input power ($L = 3\ cm$).

Figure 3.4: Representation of the TPA analytical study showing the output power varying with (a) the length and the (b) input power for a Silicon waveguide. It has been compared to the linear absorption case $P_{out} = P_{in}e^{-\alpha L}$ (red line).

In Fig. 3.4 one simulation example of such analytical comparison has been depicted for a Silicon waveguide. One could appreciate the sharp increase of losses due to nonlinear contributions in both length and power dependence. The Silicon device under estimation is characterised by $\alpha = 110\ dB \cdot m^{-1}$, $\beta_{TPA} = 5 \cdot 10^{-12}\ m \cdot W^{-1}$ and $A_{eff} = 0.1\ \mu m^2$.

Furthermore, one should examine how the known free carriers induced by the two-photon absorption are likewise limiting such power efficiency. It will be later demonstrated that this free carriers absorption (FCA) is saturating the power travelling within the device whether such power keeps increasing. Model described in Eq. 3.12 has not included this further contribution, nonetheless it will be deeply studied in the scheme presented in the following section. In order to add FCA parameters into the above method, one should start from the definition presented by [27] instead of that of Eq. 3.11.

Lastly, the present nonlinear losses mainly affecting the phase-shifting along with the power saturation has been related to another FOM so as to compare materials exhibiting two-photon absorption. Once again, related works have used different definitions for such relation.

The aforementioned figures of merit become described as

$$\frac{2\beta_{TPA}\lambda}{n_2} < 1, \tag{3.13a}$$

$$\frac{n_2}{\beta_{TPA}\lambda}. \tag{3.13b}$$

Note that the first relation [22, 23, 27–29] requires the lowest possible value in order to declare the material under comparison the best one whilst the second one [24, 26, 30] demands the opposite (i.e. the highest).

3.3 Conversion Efficiency Computation

The main tool in order to get all the media compared has been decided to be the CE parameter. Even though lots of studies have been focused on the gain characteristics, the present one has been concentrated on the wavelength conversion and, thereby, the CE coefficient. As already mentioned, DFWM is the technique considered in here in order to carry out such wavelength transformation.

First of all, working with the scheme in Fig. 2.4 under degeneracy conditions and the general definition in Eq. 2.14, the starting point for benchmark the media in terms of efficiency is declared as

$$CE_{max} = (\gamma P_p L_{eff})^2 \, e^{-\alpha L}, \tag{3.14}$$

which gives us a first approximation on how the media characteristics together with the pump power are affecting the frequency conversion. It is worth remarking that the maximum value for CE is evaluated in Eq. 3.14 where some ideal approximations have been made (e.g. no linear phase-mismatch, $\Delta k_M = 0$).

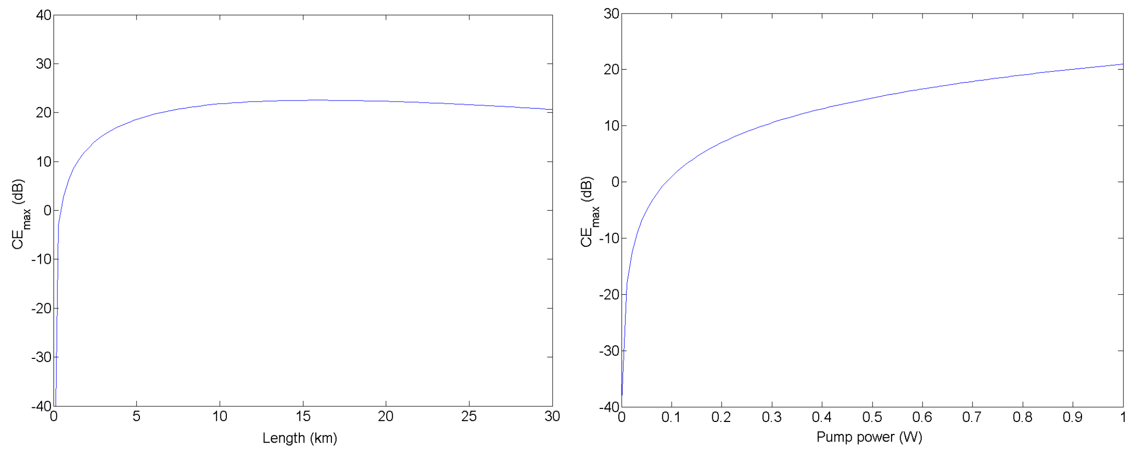

(a) Maximum conversion efficiency vs. length when $P_p = 1\ W$ is used.

(b) Maximum conversion efficiency vs. input power when $L = 8\ km$ is used.

Figure 3.5: Representation of the CE_{max} approximation varying with (a) the length (when the pump power is fixed to $1\ W$) and the (b) input power (when the length is fixed to $8\ km$) for a DSF.

In Fig. 3.5 the dependence of such maximum CE with both length and power variations has been depicted. The DSF chosen for this example is the same as in Fig. 3.2. Notice that an optimum length appears giving rise to the maximum of CE. After such an optimum point, the efficiency not only saturates but decreases. Thus, one could optimise the length by maximising the following relation extracted from Eq. 3.14

$$L_{opt} = \max_{L} \left(L_{eff}^2 e^{-\alpha L} \right), \tag{3.15}$$

which can be graphically represented as in Fig. 3.6.

Note that the maximisation condition for the length optimisation has been normalised. The case depicted in Fig. 3.6 belongs as well to the DSF example chosen in the previous estimations.
Let us move onto the power efficiency once the length has already been optimised. It is worth observing that the power optimisation in here is not fair enough since not all the parameters required in such light-matter interactions are taken into account. Nevertheless, it has introduced us into the posterior comparison by presenting a general idea on how all the media could be compared in terms of power efficiency. Such behaviour has been pictured next to the length optimisation in Fig. 3.6.

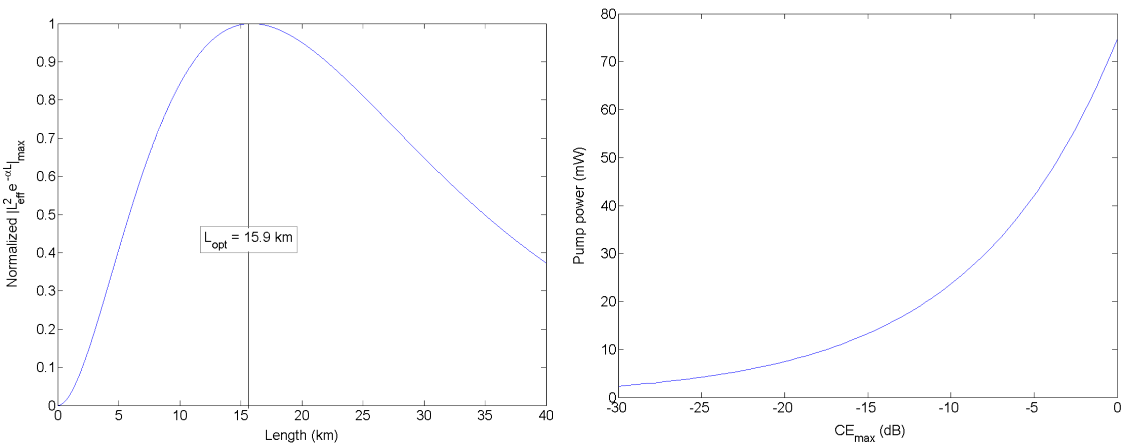

(a) Length optimisation. (b) Power requirement for a target CE_{max}.

Figure 3.6: Graphical representation of the (a) length optimisation and the subsequent (b) power efficiency for a target CE_{max}.

From now on, 4 different methods for CE computation have briefly been explained. Firstly, two well-known analytical methods give us different approximations of such efficiency computation and secondly, two numerical models bring us an accurate frequency conversion process description, with and without nonlinear losses contribution, respectively.

3.3.1 Analytical Models

In the first place, the method induced from Shibata et al. work in 1987 [31] suggests the modification of Eq. 3.14 as declared below

$$CE_{Shibata} = \left(\gamma P_p L_{eff}\right)^2 e^{-\alpha L} \eta = \eta CE_{max}, \tag{3.16}$$

where η is an efficiency parameter that behaves as

$$\eta = \frac{\alpha^2}{\alpha^2 + \Delta\beta^2} \left(1 + \frac{4e^{-\alpha L} \sin^2(\frac{\Delta\beta L}{2})}{\left(1 - e^{-\alpha L}\right)^2}\right), \tag{3.17}$$

where α and $\Delta\beta = \Delta k_M$ stand for the linear losses and the linear phase mismatch, respectively.

On the other hand, let us go five years back, in 1982, when the theory presented by Stolen and Bjorkholm [32] allowed for the following CE definition

$$CE_{Stolen} = \left(\frac{\gamma P_p}{g} \sinh(gL)\right)^2, \tag{3.18}$$

where the parametric gain coefficient is given by

$$g = \sqrt{\left(\gamma P_p\right)^2 - \left(\frac{\kappa}{2}\right)^2}. \tag{3.19}$$

The parameter κ stands for the phase mismatch.
The first computation model gives us an approximation where nonlinear phase mismatch is not considered but takes the losses into account. By contrast, the second method estimates the solutions by fully contemplating the phase mismatch (not only linear contribution), yet no losses are taken into consideration.
A comparison for both methods can be seen in Fig. 3.7 where such CE has been represented in function of signal wavelength detuning $\lambda_p - \lambda_s$.
Note that Shibata et al. model is better approaching the maximum achievable CE (i.e. considering losses, α) while Stolen and Bjorkholm model represents better the gain behaviour (i.e. considering phase mismatch effect). However, the unrealistic high values obtained by the Stolen method could be a bit more well-estimated for small detuning by considering L_{eff} instead of L, thus part of the losses effect would be regarded. The example in Fig. 3.7 belongs to a Silicon waveguide [20] characterised by $\alpha = 110\, dB \cdot m^{-1}$, $L = 10\, cm$, $\gamma = 243\, (W \cdot m)^{-1}$, $\beta_2 \approx -0.02\, ps^2 \cdot m^{-1}$ and $\beta_4 = 0$. The working point is defined by $P_p = 200\, mW$ at $\lambda = 1.55\, \mu m$.

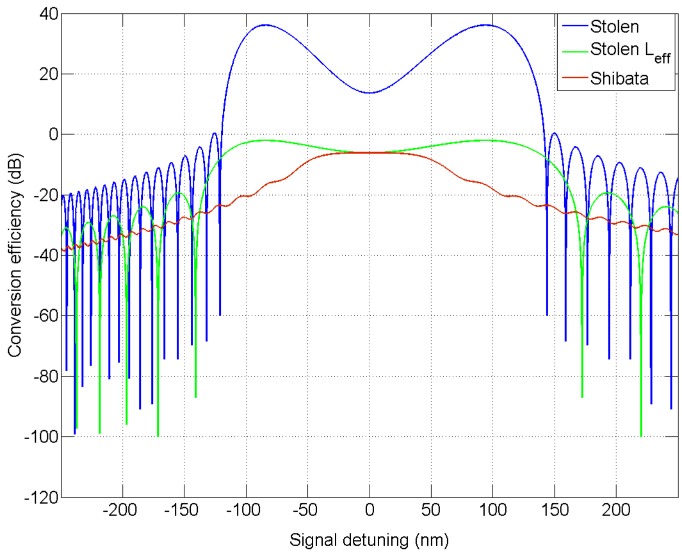

Figure 3.7: Comparison of conversion efficiency versus wavelength detuning for Shibata et al. and Stolen and Bjorkholm methods in a Silicon waveguide.

In conclusion, if we need to obtain a much more accurate response, the use of numerical methods is required. Thus, the next subsection will describe two different numerical models that give a better estimation for the desired comparison of CE.

3.3.2 Numerical Models

In this subsection the numerical models accurately studying the behaviour of all the interacting waves in the DFWM have been presented. The first method consists in simulating the field propagation along the device by solving the Nonlinear Schrödinger Equations (NLSE). Besides, the system of coupled equations presented by [33] has been utilised in this work in order to allow for nonlinear losses due to TPA and FCA.

Let us firstly present the split-step Fourier method that solves the NLSE by using a frequency sweep. That means, for every wavelength detuning the scalar value of the field propagating along the device is obtained which increases the computation time with respect to the other methods. Accordingly, either signal gain or CE can be derived. This method takes into account the effects of dispersion (κ) and linear losses (α) providing more rigorousness to the estimation. However, the model does not evaluate the output signals properly when the media presents nonlinear losses since it is not accounting for effects such as SBS, TPA or FCA. The computation process is thoroughly detailed in [1, 21]. This method is graphically represented by an example in Fig. 3.8
One could appreciate that linear losses are affecting the maximum reachable CE level (as in Shibata et al. model) whilst parametric gain behaviour is still being exhibited owing to the phase mismatch contribution (as in Stolen and Bjorkholm model).

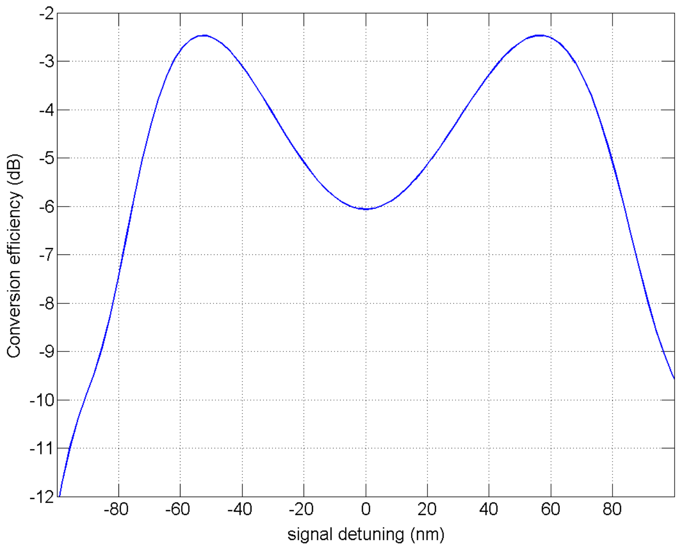

Figure 3.8: Conversion efficiency versus wavelength detuning for the split-step Fourier method in a Silicon waveguide.

On the other hand, a model that includes nonlinear losses due to TPA and FCA in the DFWM scheme is required for a much more meticulous comparison. Consequently, the set of coupled equations revealing the effects resulting from TPA (α_{TPA}), TPA-induced FCA (α_{FCA}) and linear phase mismatch ($\Delta\beta = \Delta k_M$) has been employed. Hence, the system can be expressed as

$$\frac{dA_p}{dz} = -\frac{1}{2}(\alpha + \alpha_{TPAp} + \alpha_{FCAp})A_p + j\gamma\left[|A_p|^2 + 2|A_s|^2 + 2|A_i|^2\right]A_p + 2j\gamma A_p^* A_s A_i e^{j\Delta\beta z} \tag{3.20a}$$

$$\frac{dA_s}{dz} = -\frac{1}{2}(\alpha + \alpha_{TPAs} + \alpha_{FCAs})A_s + j\gamma\left[2|A_p|^2 + |A_s|^2 + 2|A_i|^2\right]A_s + j\gamma A_i^* A_p^2 e^{-j\Delta\beta z} \tag{3.20b}$$

$$\frac{dA_i}{dz} = -\frac{1}{2}(\alpha + \alpha_{TPAi} + \alpha_{FCAi})A_i + j\gamma\left[2|A_p|^2 + 2|A_s|^2 + |A_i|^2\right]A_i + j\gamma A_s^* A_p^2 e^{-j\Delta\beta z} \tag{3.20c}$$

where A_j denotes the amplitude of the interacting waves ($j = p, s, i$ for the pump, signal and idler, respectively) propagating along the distance z, α the linear losses, α_{TPA_j} and α_{FCA_j} stand for the nonlinear losses coefficients due to TPA and FCA, respectively, γ is the nonlinear coefficient and $\Delta\beta = \Delta k_M$ refers to the linear phase mismatch parameter. Specifically, such nonlinear losses can be clearly stated as

$$\alpha_{TPAj} = \frac{\beta_{TPA}}{A_{eff}}\left(|A_j|^2 + 2\sum_{m\neq j}|A_m|^2\right) \tag{3.21}$$

$$\alpha_{FCAj} = \frac{\sigma\beta_{TPA}\tau}{2hcA_{eff}^2}\left(\sum_m \lambda_m|A_m|^4 + 4\sum_{m\neq n}\frac{\lambda_m\lambda_n|A_m|^2|A_n|^2}{\lambda_m + \lambda_n}\right) \tag{3.22}$$

($j = p, s, i$ for the pump, signal and idler waves)

where β_{TPA} indicates the TPA coefficient, A_{eff} the effective area, σ designates the FCA cross section and τ the carriers lifetime. Notice that α_{TPA} directly increases with the incident power while α_{FCA} is quadratically proportional to that power since $P_j \approx |A_j|^2$. Similar to the previous numerical solution, by solving the system in Eq. 3.20 all the fields ($A_k(z)$) has been defined and thereby, the powers at the output which permits us to calculate the CE by means of Eq. 2.14. It is worth remarking that this method is valid under the CW assumption. It has graphically been represented an example for this method in Fig. 3.9.

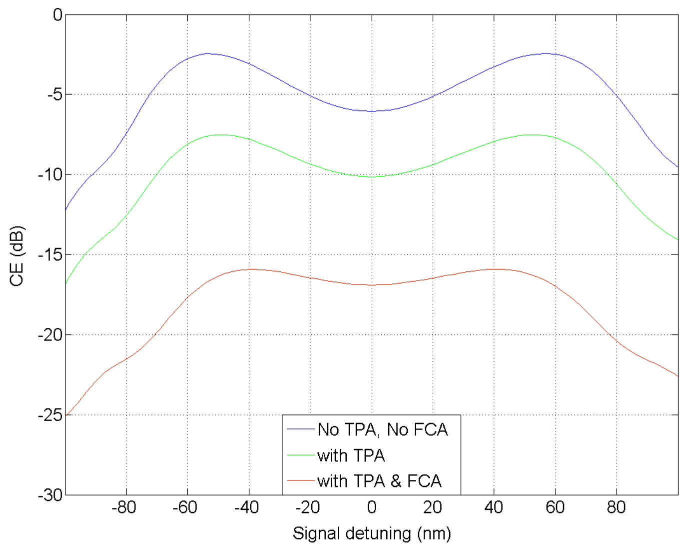

Figure 3.9: Conversion efficiency versus wavelength detuning for the coupled equations method in a Silicon waveguide.

Three different cases have been exemplified in Fig. 3.9 where either absence of nonlinear losses (blue curve), only TPA (green curve) or both TPA and FCA (red curve) assumption is supposed. It can be seen how the raise in losses due to TPA and FCA notably reduces the CE. Even though linear phase mismatch has solely been considered, the estimation is in good agreement with the split-step Fourier method. The simulations have been made considering the same Silicon waveguide utilised above.

3.4 Comparison Procedure

In this section we are going to describe the procedure performed in this study in order to compare the different nonlinear materials. It is based on an optimising process in terms of power requirement and the device length. Correspondingly, the minimum power needed for a target CE will be investigated via the coupled equations method presented in the end of the previous section.

As aforementioned, the benchmark presented in here focuses on the estimation of the maximum achievable CE in a DFWM scheme. Hence, such parameter defined in Eq. 2.14, which compares the idler power at the output to the signal power at the input of a waveguide, has been computed using the system in Eq. 3.20. It is worth remarking that for such comparison linear phase matching has been considered ($\Delta\beta = \Delta\kappa_M = 0$) so as to expect the maximum CE together with the signal power of $P_s = 1\,mW$.
First of all, we need to present the result for the estimation of the CE vs. both power and length parameters.

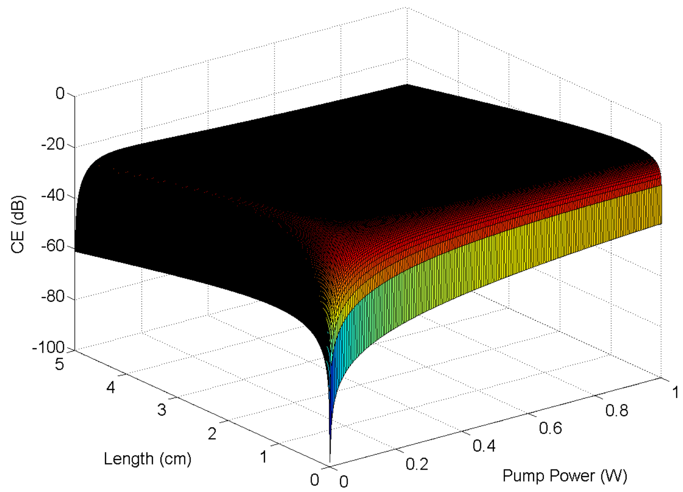

Figure 3.10: Conversion efficiency versus pump power and length for the coupled equations method in an amorphous-Silicon waveguide.

In Fig. 3.10 one could observe the variation in CE that both parameters, input power and length, are inducing. In the depicted example we have considered an amorphous-Silicon waveguide characterised by $\alpha = 450\,dB \cdot m^{-1}$, $\gamma = 1200\,(W \cdot m)^{-1}$, $\beta_{TPA} = 2.5 \cdot 10^{-12}\,m \cdot W^{-1}$, $A_{eff} = 0.07\,\mu m^2$, $\sigma_{FCA} = 1.9 \cdot 10^{-20}\,m^2$ and $\tau_{FCA} = 400\,ps$ (see Table 4.1).
Another computational step is needed in order to clarify such behaviour. The information contained in Fig. 3.10 is mathematically represented by

$$CE_{m,n} = \begin{pmatrix} CE_{1,1} & CE_{1,2} & \cdots & CE_{1,n} \\ CE_{2,1} & CE_{2,2} & \cdots & CE_{2,n} \\ \vdots & \vdots & \ddots & \vdots \\ CE_{m,1} & CE_{m,2} & \cdots & CE_{m,n} \end{pmatrix}$$

where each row contains the CE values for a certain pump power, $P_p \in [0,1]\ W$, while varying the length, $L \in [0,5]\ cm$. The optimisation premise from that CE matrix has been stated as

$$P_{opt} = \{P_{p_{min}} \,|\, CE_{m,n} = X\ dB\}\,, \tag{3.23}$$

meaning that, the minimum power required to reach a certain CE target value will decide the optimum couple $[P_{opt}, L_{opt}]$. This optimising determination has graphically been represented so as to facilitate the comprehension. Hence, the contour lines from the 3D-plot (see Fig. 3.10) have been pictured so that one could appreciate the variations in a much more perceptible manner together with the optimising process on it.

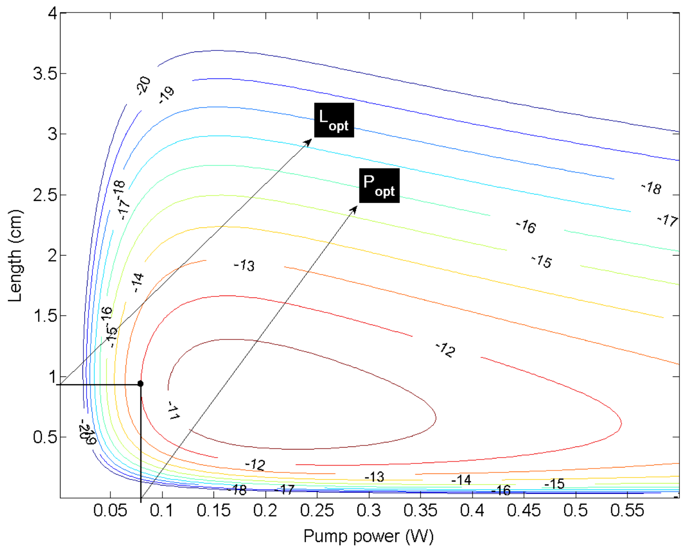

Figure 3.11: Conversion efficiency contour levels $[-20, -10]$ dB versus pump power and length for the coupled equations method in an amorphous-Silicon waveguide. The optimisation process has also been presented for the level of $CE = -12\ dB$ indicating the minimum pump power, P_{opt}, and the corresponding optimum length, L_{opt}.

Consequently, the minimum pump power required for each target CE could be defined. This final step of the procedure is basically the comparison and it will be seen in the next Chapter 4.

3.5 Summary

To sum up, this chapter has been divided into 4 different sections plus this summarising part. Each of them has presented different tools intended for the estimation of nonlinear effects originated in different media.

- Firstly, some SBS characteristics has been described together with two methods. The first one gives an analytical approximation of the threshold power in some materials while the second one is numerically evaluating the field propagation along the device.

- Secondly, the analogous characterisation has been made for the TPA phenomenon, where an analytical method to obtain the power efficiency is exemplified.

- Thirdly, different models for the CE computation are provided. Whereas the first two models consist of an analytical estimation of such parameter, the other two models numerically calculate the field components giving a much more accurate result. It is worth commenting that the last numerical method allowing for nonlinear losses contributions will be used for precise comparison while some of the results will be corroborated by using the split-step frequency sweep calculation, where the dispersion effects are meticulously examined.

- Finally, the optimising procedure is detailed in the fourth section. It will be used for the different selected media in the next Chapter 4.

CHAPTER 4

Simulation Results: Comparison of Nonlinear Media

This chapter will guide the reader through different results obtained by means of some of the tools previously presented. Different analytical and numerical models have been used so as to analyse different nonlinear media when phenomena such as SBS, TPA or FCA are participating. Moreover, the case study considered in this work in order to obtain a benchmark for the materials consists of a wavelength conversion through the degenerate case (DFWM) with $\lambda_p = 1.55\,\mu m$ ($f_p = 193\,THz$ in Fig. 2.4). Accordingly, some numerical and graphical outcomes containing information about nonlinear effects will be presented. Matlab® software has been used for such computations.

First of all, it is noteworthy that an important part of this thesis has been dedicated to literature review. Therefore, an exhaustive research has been carried out in order to classify different nonlinear media examined beforehand in the related work. The main parameters taken into account in such classification are the nonlinear refractive index, n_2, the nonlinear coefficient, γ, the linear losses, α, the effective area, A_{eff}, and respectively the SBS gain coefficient and the TPA coefficient, g_B and β_{TPA}. In addition, the FCA-cross section, σ_{FCA}, and the carrier lifetime, τ, become important in case the efficiency turns to be diminished by the FCA.
Hence, in Table 4.1 we have listed a wide variety of nonlinear media that we found to be promising in the field of nonlinear optics throughout the research.

From Table 4.1 we will compare some of the media in order to understand how the nonlinear phenomena modify the efficiency in the process of wavelength conversion by means of DFWM. Notice that some materials will not be taken into consideration for such comparison since few properties were missing. In the first two sections some of the fibres have been analysed starting from the Silica high-nonlinear fibre (HNLF), followed by the

Material	Properties of Nonlinear Media							Ref.
	n_2 $\left(\frac{m^2}{W}\right)$	γ $\left(\frac{1}{W \cdot m}\right)$	D $\left(\frac{ps}{km \cdot nm}\right)$	α $\left(\frac{dB}{m}\right)$	A_{eff} $\left(\mu m^2\right)$	g_B $\left(\frac{m}{W}\right)$	β_{TPA} $\left(\frac{m}{W}\right)$	
Silica HNLF	4.2×10^{-20}	11.5×10^{-3}	-0.1	8.3×10^{-4}	11	7.9×10^{-12}	-	[20, 34]
Bi_2O_3 HNLF	8.2×10^{-19}	1.1	-260	0.8	3.1	6.43×10^{-11}	-	[20]
As_2S_3 HNLF	2×10^{-18}	0.16	410	0.88	5	6.1×10^{-9}	6.2×10^{-15}	[35]
As_2Se_3 HNLF	1.1×10^{-17}	1.2	-504	1	37	6×10^{-9}	2.5×10^{-12}	[35]
As_2S_3 WG	2.9×10^{-18}	1.7	-342	5	6.9	-	6.2×10^{-15}	[35]
As_2Se_3 HNLF taper	1.1×10^{-17}	93.4	282	1	0.5	-	2.5×10^{-12}	[35]
As_2S_3 disp-engin. WG	3×10^{-18}	9.9	29	60	11	-	6.2×10^{-15}	[35]
$Ge_{11.5}As_{24}Se_{64.5}$ nanowire	9×10^{-18}	136	70	250	0.3	-	1×10^{-13}	[35]
Ag-As_2Se_3 PhC WG	7×10^{-17}	2.6×10^4	-	1×10^3	1.1×10^{-2}	-	-	[35]
Lead-Silicate ($SF57$) HF	4.1×10^{-19}	0.82	-4	2.1	2	-	-	[36]
Tellurite HNLF	2.5×10^{-19}	0.110	-	5.4×10^{-2}	9.2	1.47×10^{-10}	-	[19]
Silica Holey Fibre	8.9×10^{-20}	56.2×10^{-3}	38	1.2×10^{-2}	6.4	1.33×10^{-11}	-	[20]
Silica DSF	2.6×10^{-20}	2.4×10^{-3}	-1.6	3×10^{-4}	44	6.17×10^{-12}	-	[20]
GeO_2-SiO_2 HNLF	3.3×10^{-20}	11.6×10^{-3}	-6×10^{-2}	8.3×10^{-4}	11.5	3.02×10^{-12}	-	[16]
Al-SiO_2 HNLF	2.5×10^{-20}	7.4×10^{-3}	-0.35	1.5×10^{-2}	13.5	1.41×10^{-12}	-	[16]
AlGaAs WG	1.43×10^{-17}	10	-910	200	5.7	-	5×10^{-13}	[37]
Hydex® WG	1.1×10^{-19}	0.22	-	6	2	-	-	[38]
Si_3N4 WG	9×10^{-20}	0.2	-	3	1.8	-	-	[39]
crystalline-Silicon WG	6×10^{-18}	243	-	110	0.1	-	5×10^{-12}	[40, 41]
amorphous-Silicon WG	2.1×10^{-17}	1200	330	450	7×10^{-2}	-	2.5×10^{-12}	[42, 43]

Table 4.1: List of properties for different nonlinear media at the telecommunications band ($\lambda_p = 1.55\ \mu m$). Different structures such as fibres, waveguides and nanowires have been presented. Parameters describing SBS and TPA contributions have been gathered whereas FCA characteristics (for Silicon devices) have been excluded from the Table.

Bismuth (Bi_2O_3) HNLF and finally, these two fibres will be compared to other nonlinear HNLFs that exhibit SBS effects as well. Afterwards, some of the waveguides structures will likewise be examined. Whether TPA and FCA deteriorate the efficiency or not will also be observed in such sections. After all, a general comparison between all the selected media will be presented in the last section.

4.1 Silica High-Nonlinear Fibre

One could assert that Silica (SiO_2) HNLFs have mostly been employed throughout many years in nonlinear optics (NLO). Amongst other properties, Silica HNLFs present extremely low linear losses and dispersion controllability [44] allowing for high parametric gain within a wide wavelength range. Nevertheless, the launched power must be limited in many cases due to nonlinear losses coming from SBS. Thus, some techniques must be performed so as to suppress such effect.

Moving on to the analysis, it has been observed that Silica HNLFs do not present any symptom of nonlinear losses resulting from neither TPA nor FCA. However, the efficiency of such devices could be heavily decreased owing to the scattering losses emerging from SBS. Hence, the field propagation along the Silica HNLF has been studied considering the fact that SBS is limiting the CE.
Firstly, an analytical study has been done for the Silica fibre listed in Table 4.1 in order to

get a general idea for the threshold power. In addition, the corresponding figure of merit (FOM) will be provided by means of Eq. 3.8. Whether the threshold power due to the SBS phenomenon is defined as in Eq. 3.7 the fibre length could be affecting such threshold as depicted in Fig. 4.1.

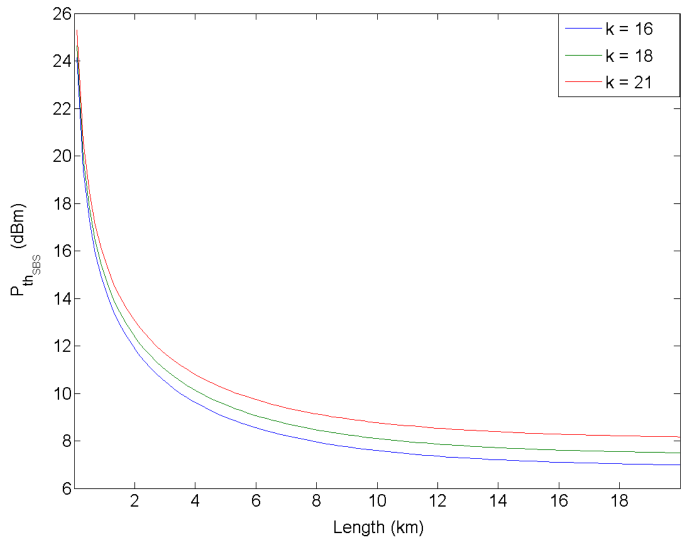

Figure 4.1: Stimulated Brillouin Scattering threshold power (SBST) varying with length in a Silica HNLF. Three different cases has been presented with $k = 16, 18$ and 21, respectively.

One could observe the sharply decreasing behaviour for the threshold power SBST while augmenting the length of the fibre. However, after a few kilometres, the threshold does not decrease so intensively. It is worth mentioning that unlike other typical values of g_B for Silica HNLF [1], this fibre presents a Brillouin gain one order of magnitude lower, $g_B = 7.19 \cdot 10^{-12}\, m \cdot W^{-1}$. Hence, SBST values are quite higher than usual (e.g. $P_{th} \approx 9.8\, dBm$ for a fibre length of $6\, km$ when the factor $k = 21$ in Eq. 3.7). Consequently, by means of Eq. 3.8 the FOM for this concrete Silica HNLF is

$$FOM_{SBS} = 0.366.$$

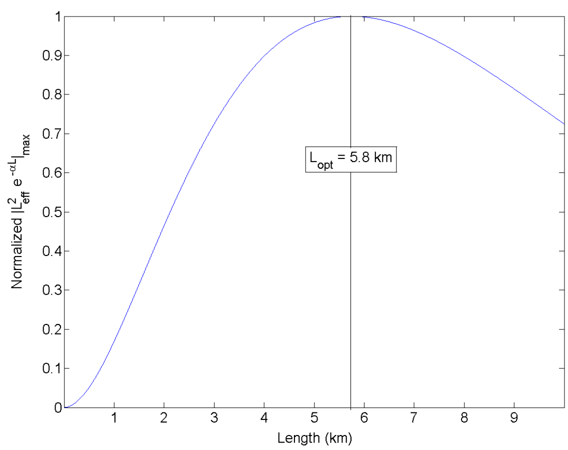

Figure 4.2: Optimum length by means of linear losses optimisation in the present Silica HNLF.

Secondly, and much more accurate, the aforementioned numerical method has been applied. It is worth recalling that the coupled equations described in Eq. 3.10 has been solved by the use of a shooting algorithm. Moreover, for such solution, the specific device length is needed thus, we have followed the optimisation procedure stated in Eq. 3.15. The CE maximisation in terms of the linear losses, α, brings the optimum length as depicted in Fig. 4.2.

Accordingly, the Silica HNLF of $5.8\ km$ has numerically been examined in order to display the SBS effect involved in the field propagation. For such goal, the input pump power (P_p) and the Stokes power (P_S) propagating along the fibre will be illustrated when the former (P_p) keeps increasing. Those behaviours are pictured in Fig. 4.3.
It can be seen from Fig. 4.3 that the wave travelling forwards is being nonlinearly decreased due to the scattering losses coming from the SBS effect when the input pump power overcome some threshold.

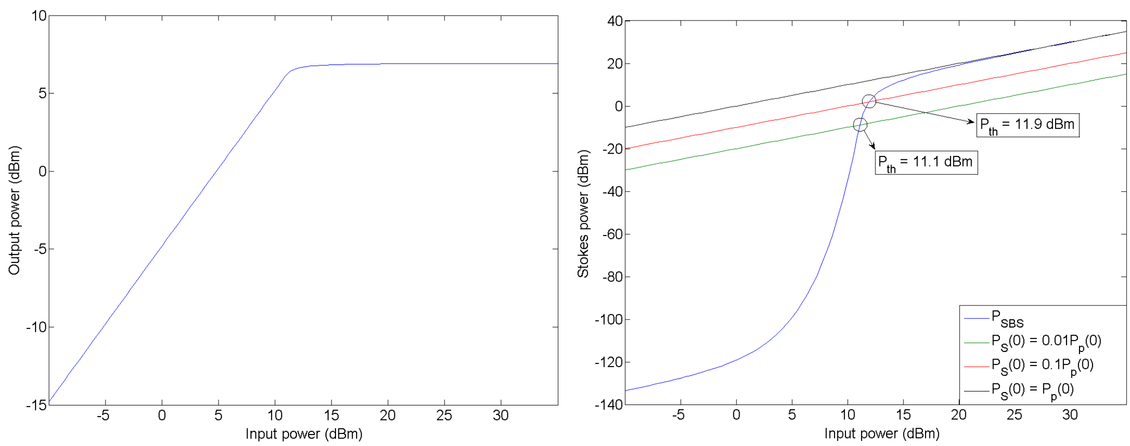

(a) Output power vs. Pump power.　　(b) Stokes power vs. Pump power.

Figure 4.3: Graphical representation of the (a) output power and the (b) Stokes power in a Silica HNLF when the input power keeps increasing.

For the purpose of deciding the SBST, the relation defined in Eq. 3.6 with $\mu = 0.01, 0.1$ and 1 has been plotted. The resultant intersections with the Stokes curve settle the so-called SBST for each case. Notice that the less restrictive condition ($\mu = 1$) settles the SBST at a power higher than those represented in the picture. Henceforth, the more restrictive condition ($\mu = 0.01$) will be chosen giving rise to a threshold power and a FOM of

$$P_{th} = 12.9\, mW\ (11.1\, dBm) \quad \rightarrow \quad FOM_{SBS} = 0.522.$$

Compared to the analytically calculated value, when $k = 21$ and $L = 5.8\, km$, the threshold obtained by means of the numerical computation is $1.3\ dB$ higher.

On the other hand, the analysis that will essentially be the comparison, consists in representing the minimum pump power required to attain each maximum CE. The method employed in here has been explained in the previous Chapter 3. Therefore, considering the model of the coupled equations described in Eq. 3.20 such power evolution has been pictured in Fig. 4.4.

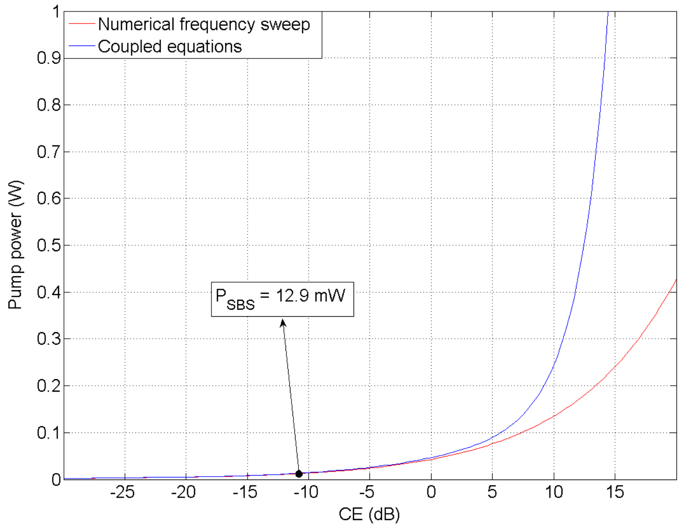

Figure 4.4: Graphical representation of the minimum pump power (optimum) versus the target CE for a Silica HNLF. It has been included the computation using the split-step frequency sweep model.

The power optimisation depicted in Fig. 4.4 shows the minimum input power required for each CE computed by the two numerical models. Not in the following cases but in this one (Silica HNLF), the relation obtained for efficiencies higher than 5 dB (approximately) with the coupled equations model is not trustworthy thus, the split-step computation has been included. It is worth remarking that the device length is not being affected by the nonlinear losses, so the optimum length coincides with that calculated before by maximising the product $L_{eff}^2 e^{-\alpha L}$. Hence, the length of 5.8 km stands for the optimum length in the present case.

However, one should take into account that fibres of such a long length are not used in practice since the polarisation instability notably increases which leads to a rise in losses. Furthermore, phase matching can be challenging in long devices, so $\Delta\beta = 0$ would not be longer accomplished. Hence, one of the goals could be the spatial optimisation of the device. Note that neither polarization nor dispersion changes along the fibre have been contemplated in here.

If one pays attention to Fig. 4.4 will observe that SBST has been pointed in the curve. It reminds that, although Silica HNLFs provide a good performance in the wavelength conversion process, whether no countermeasure is used to suppress the SBS effect, the efficiency could become drastically deteriorated.

4.2 Bismuth Oxide High-Nonlinear Fibre

Even though Silica HNLFs present a good behaviour in the frequency conversion application, they are limited by a relatively modest Kerr nonlinearity. In the current section an n_2-enhanced material will be likewise analysed. The nonlinear device in question consists of a bismuth oxide (Bi_2O_3) HNLF, which presents a much greater gamma coefficient ($\gamma = 1.1 \ (W \cdot m)^{-1}$) than that of Silica.

Analogous to the case of Silica, no nonlinear losses coming from TPA, and hence, nor from TPA-induced free carriers (FCA) have been noticed in this bismuth fibre. Yet, SBS could be diminishing the efficiency of the process at high input powers. Thus, the following behaviour depicted in Fig. 4.5, analytically obtained, describes in a general view the SBS impact to the fibre.

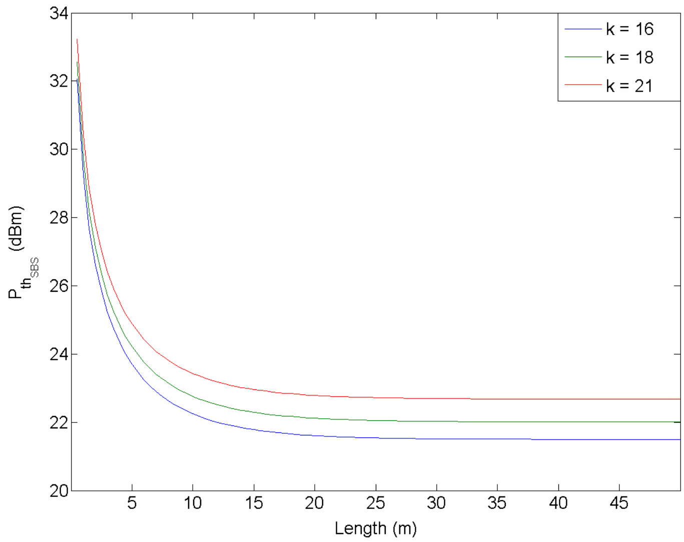

Figure 4.5: Stimulated Brillouin Scattering threshold power (SBST) varying with length in a Bi_2O_3 HNLF. Three different cases has been presented with $k = 16, 18$ and 21, respectively.

Note that even its higher Brillouin gain ($g_B = 6.43 \cdot 10^{-11} \ m \cdot W^{-1}$), the SBST for the bismuth HNLF is higher than that of Silica. This is because of its higher linear losses ($\alpha = 0.8 \, dB \cdot m^{-1}$) that force to use shorter devices. Such threshold (with $k = 21$) for this material and its corresponding FOM for a fibre length of 6 m are equal to

$$P_{th} = 277.3 \, mW \ (24.4 \, dBm) \quad \rightarrow \quad FOM_{SBS} = 1.11$$

One could observe that the SBST for the bismuth HNLF is much higher than that of the Silica one ($P_{th_{Bismuth}} \approx 21 \times P_{th_{Silica}}$) while the FOM is about 2 times greater.

It is not recommended (in terms of losses optimisation) to use more than 6 m of Bismuth fibre for the wavelength conversion process in a DFWM, otherwise the linear losses will become more and more important thus, rapidly decreasing the CE. It can be extracted (analogously to the Silica case) from the length optimisation in Eq. 3.15.

Besides, the pump and the Stokes signals interaction can be detailed by the plots in Fig. 4.6. Again, the inelastic process (SBS) inducing backscattered power across the nonlinear media has been described versus the increase of the input power for the Bismuth case study.

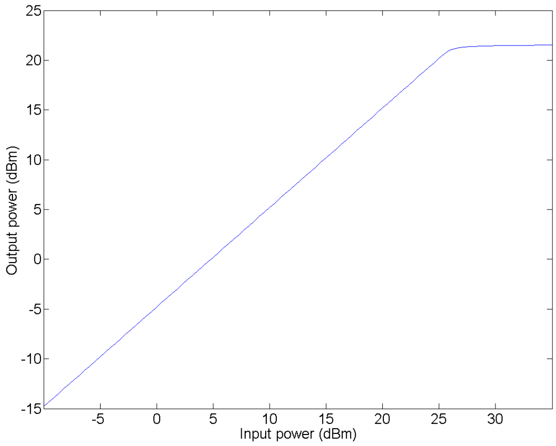

(a) Output power vs. Pump power.

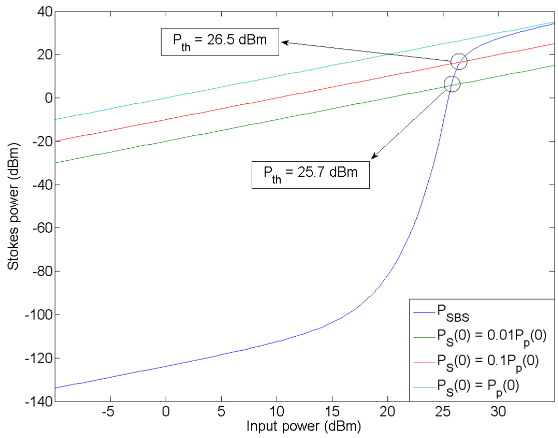

(b) Stokes power vs. Pump power.

Figure 4.6: Graphical representation of the (a) output power and the (b) Stokes power in a Bismuth HNLF when the input power keeps increasing.

The numerically estimated threshold for the Bismuth fibre considering the restriction $\mu = 0.01$ (i.e. 1% of the pump power backscattered) and its FOM turn out to be

$$P_{th} = 373.3\, mW\ (25.7\, dBm) \quad \rightarrow \quad FOM_{SBS} = 1.49$$

which is $1.3\, dB$ higher than the analytical estimation as occurred in the Silica HNLF.

Let us now move on to the CE computation utilising the system defined by the set of coupled equations. In this second (Bismuth) fibre, the corroboration from the split-step Fourier method has not been necessary. Hence, such power minimisation has been pictured in Fig. 4.7.

This scheme brings us a pretty good performance still at not so high powers because of the high nonlinear coefficient (γ) together with the relatively low linear losses (α). Nonetheless, one should remind the effect of SBS in the fibre, which could entail a notable reduction of the power efficiency. Actually, in the case of bismuth fibre, it does present a higher threshold but still not allowing for powers higher than $450\, mW$ which would imply positive efficiencies (i.e. gain). Though, some techniques such as core-doping or multi-segmenting the fibre [10] can be applied so as to suppress (or lessen) the SBS effect.

By way of comparison, let us present both the analytical and the numerical SBST results obtained for the different materials declared in Table 4.1 exhibiting the SBS phenomenon.

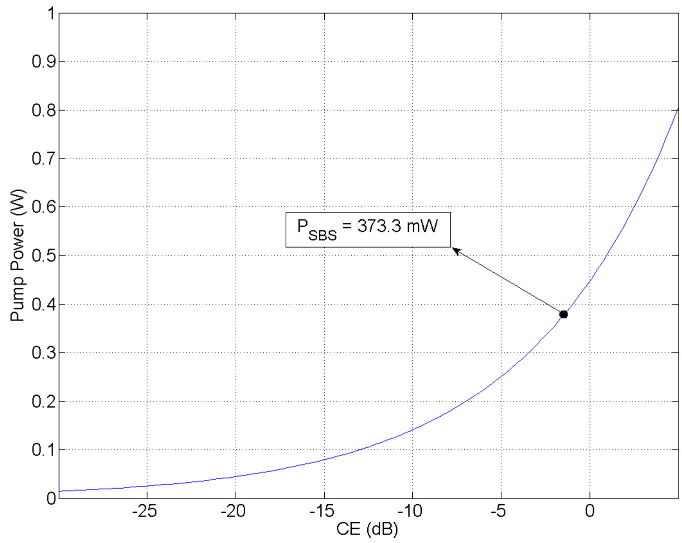

Figure 4.7: Graphical representation of the minimum pump power (optimum) versus the target CE for a Bismuth HNLF.

Firstly, the Table 4.2 shows us the comparison for the analytical formulation considering $k = 21$ and the respective optimum lengths for each media by means of maximising $L_{eff}^2 e^{-\alpha L}$.

Analytical Comparison				
Material	L_{opt} (m)	L_{eff} (m)	P_{th} $(mW)/(dBm)$	FOM
SiO_2 HNLF	5748	3488.2	9.2 (9.64)	0.369
Bi_2O_3 HNLF	6	3.6	277 (24.43)	1.1
As_2S_3 HNLF	6	3.5	5 (6.95)	3×10^{-3}
As_2Se_3 HNLF	4	2.6	49.5 (16.95)	0.154
Tellurite HNLF	88	53.5	24.6 (13.9)	0.145
SiO_2 HF	398	241.4	41.9 (16.22)	0.568
SiO_2 DSF	15904	9651	15.5 (11.91)	0.359
$Ge - SiO_2$ HNLF	5748	3488.2	22.9 (13.6)	0.927
$Al - SiO_2$ HNLF	318	193	1041.8 (30.18)	1.488

Table 4.2: Comparison by means of the analytical estimation between different fibres. The threshold (P_{th}), in both mW and dBm, and the figure of merit (FOM) have been stated together with the optimum and the corresponding effective lengths, L_{opt} and L_{eff}, respectively.

It is worth remarking that the optimum length for the Silica HNLF presented in the previous section, has been approximated to 5.8 km whilst it should precisely be a bit shorter as seen in Table 4.2.

The comparison in terms of both SBST and FOM has been made in order to reflect that a higher FOM does not necessarily mean a better threshold. Chalcogenide fibre made of As_2S_3 is not presenting a good performance in terms of SBS threshold however, it will be observed that in a waveguide scheme it is a promising material. It can be clearly observed that core-doping (Germanium and Aluminium) decreases the SBS effect in terms of power efficiency. In conclusion, the two best solutions seem to be $Al - SiO_2$ and Bismuth fibres. The trade-off between them lies in the length-power optimisation, since the former shows a higher SBST but the second allows for shorter devices. In this work the Bismuth fibre has been selected owing to its higher nonlinear coefficient (γ).

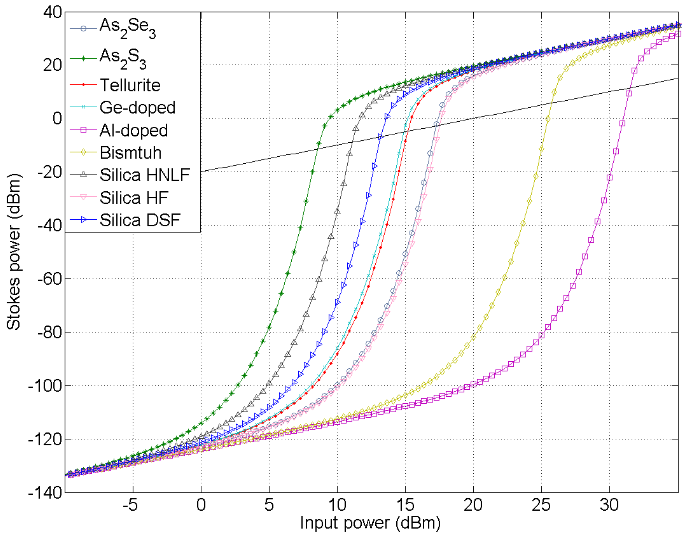

Figure 4.8: Graphical representation of the Stokes power versus the input power for different HNLFs. The condition of $P_S(0) = 0.01 \cdot P_p(0)$ has been traced to visualise the SBST.

On the other hand, the numerical comparison between these nonlinear media has graphically been presented. The result can be observed in Fig. 4.8, where the evolution of the output and the backscattered (Stokes) powers have been pictured while varying the input power. The threshold powers acquired by the numerical procedure are listed down in Table 4.3.

From now on, the comparison for the waveguide structures will be reported in the next sections. The waveguides chosen for the comparison are those composed of materials with enhanced nonlineariteis such as high-index doped Silica (Hydex ®), Silicon Nitride (Si_3N_4), Chalcogenide glass (As_2S_3), the alloy made of Aluminium-Gallium-Arsenic (AlGaAs) and finally, the crystalline and amorphous Silicon compounds, $c - Si$ and $a - Si$, respectively.

4.3 Hydex ® and Silicon Nitride (Si_3N_4) Waveguides

The waveguides comparison is essentially the same as the previous one realised for the fibres consisting in minimising the required power for a target CE. In the group of waveguide structures the phenomenon of SBS is no longer affecting hence, no power

Numerical Comparison	
Material	P_{th} $(mW)/(dBm)$
SiO_2 HNLF	12.94 (11.12)
Bi_2O_3 HNLF	374.11 (25.73)
As_2S_3 HNLF	7.16 (8.55)
As_2Se_3 HNLF	53.09 (17.25)
Tellurite HNLF	33.04 (15.19)
SiO_2 HF	56.49 (17.52)
SiO_2 DSF	20.84 (13.19)
$Ge - SiO_2$ HNLF	30.83 (14.89)
$Al - SiO_2$ HNLF	1402.8 (31.47)

Table 4.3: Comparison by means of the numerical estimation between different fibres. The threshold (P_{th}), in both mW and dBm, has been stated.

limitation will emerge from such effect. Nevertheless, in some cases the effects coming from TPA and/or FCA will be the limiting factors.

Let us focus on the first couple which consists of Hydex® and Si_3N_4 waveguides. The particularity of these devices is that none of the nonlinear losses presented in this thesis is affecting the performance. Hence, the comparison will be made directly looking at the power optimisation procedure. First of all, one can see in Table 4.1 that both media present similar linear losses resulting in the optimum lengths depicted in Fig. 4.9.

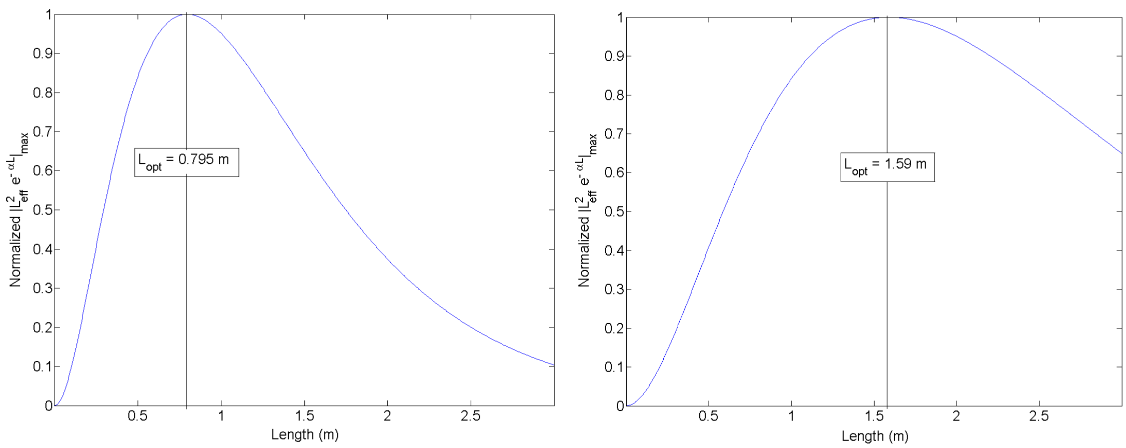

(a) Hydex. (b) Silicon Nitride.

Figure 4.9: Length optimisation in terms of linear losses ($L_{eff}^2 e^{-\alpha L}$) for the (a) Hydex® and the (b) Silicon Nitride waveguide.

Once the devices lengths are estimated to be $79.5\ cm$ and $1.59\ m$ respectively for the Hydex® and the Si_3N_4, we can carry on with the analysis of the system described in Eq. 3.20. The set of coupled equations has been solved giving rise to the CE computation and thus, the optimisation procedure (declared in the previous Chapter 3) provided the relation between the minimum power required and the CE in the wavelength conversion process as illustrated in Fig. 4.10.

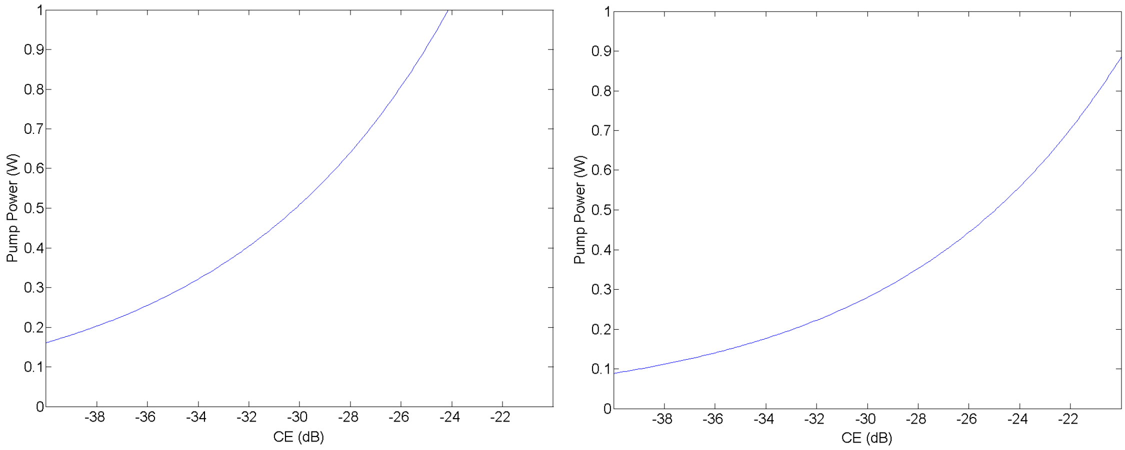

(a) Hydex.

(b) Silicon Nitride.

Figure 4.10: Power minimisation representation. The minimum pump power required for a target CE in a (a) Hydex® and a (b) Silicon Nitride waveguides.

Even though Hydex® exhibits a little bit greater (γ), the lower linear losses (α) in the Silicon Nitride device allow for a better performance. Notice that at the same pump power, the maximum attainable CE in the Si_3N_4 is approximately $5\ dB$ higher than that of Hydex®. In addition, one could assert that an extra amplifier will be needed in order to get either transparency or gain ($P_i(L) \geq P_s(0)$) because of the low efficiency achievable in these structures within the range of $1\ W$ of pump power. This power range is considered to be more than acceptable since higher powers would not provide a fair comparison. Furthermore, we must recall the assumption of CW scheme hence, high powers could become harmful for some of the media.

4.4 AlGaAs and Chalcogenide ($\mathbf{As_2S_3}$) Waveguides

In this second group two different materials are investigated. The reason to gather this pair of devices is that the literature reported TPA coefficients for the two of them. Notwithstanding, the nonlinear losses resulting from TPA turn out to be insignificant in our CE computations. No free carriers are induced by the TPA so no FCA repercussions appear in the system.

Chalcogenide glass fibre has presented a bad performance if no countermeasure is used to suppress the SBS however, this section is providing another scheme for the As_2S_3 that will show a totally different performance in terms of frequency conversion efficiency. AlGaAs is one of the media which has recently raised interest in nonlinear optics since really high nonlinear coefficients seem to be feasible in the near future.

The analytical comparison previously stated for the TPA effect is not helpful in this two designs because accounting for nonlinear losses shows no difference in the behaviour. Hence, the procedure analogous to the one of the previous waveguides has been performed. On the one hand, the optimum length for both structures is extracted from Eq. 3.15 as outlined in Fig. 4.11.

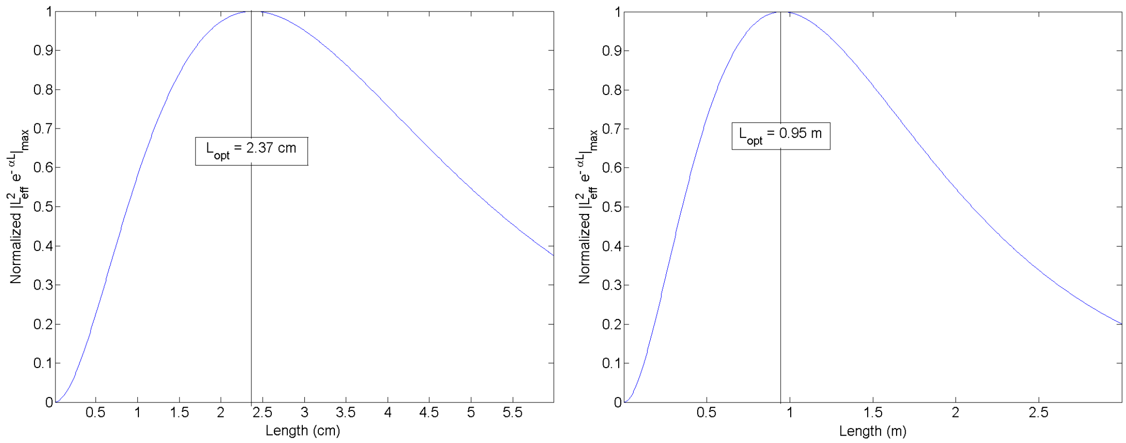

(a) AlGaAs. (b) Chalcogenide.

Figure 4.11: Length optimisation in terms of linear losses ($L_{eff}^2 e^{-\alpha L}$) for the (a) AlGaAs and the (b) Chalcogenide waveguides.

Note that the difference of two order of magnitude in the linear losses factor (α) between them results in two different structures, allowing lengths of $2.37\ cm$ and $0.95\ m$ for the AlGaAs and the As_2S3 waveguides, respectively. On the other hand, the efficiency for such devices will be provided in order to benchmark the two media in terms of power requirement. Therefore, the graphical representation in Fig. 4.12 displays such power optimisation for the maximum achievable CE.

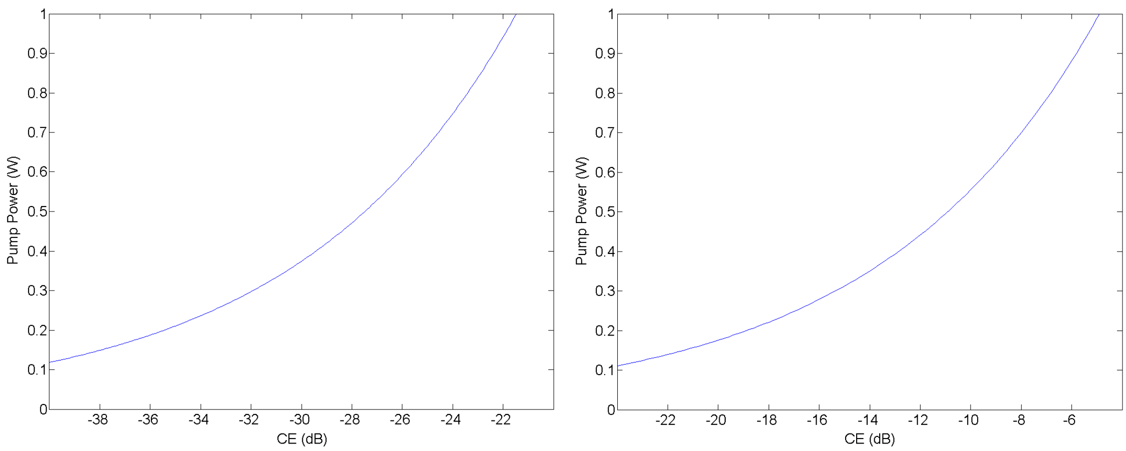

(a) AlGaAs. (b) Chalcogenide.

Figure 4.12: Power minimisation representation. The minimum pump power required for a target CE in an (a) AlGaAs and a (b) Chalcogenide waveguides.

The almost 6 times better nonlinear gamma (γ) for the AlGaAs design has not resulted in a better performance. Comparatively to the last two waveguides benchmarking, the deciding factor in the power minimisation has been the linear losses (α) which are much more important for the AlGaAs. Hence, about $16\ dB$ of improvement (with respect to AlGaAs) in the frequency conversion efficiency is accomplished by the As_2S_3 waveguide. It must be remarked that despite higher powers in the Chalcogenide waveguide might end in positive efficiencies ($CE > 0\ dB$), it could become harmful.

In the same research group, my colleague Jaume Bohigas [45] has simultaneously realised a deeper study on the III-V materials (AlGaAs and InGaP). By optimising an $Al_{0.18}Ga_{0.82}As$ (and BCB cladding) waveguide structure, the simulation results have provided efficiencies up to $11.3\ dB$ whether $\Delta\beta = 0$. When total phase matching was considered ($\kappa = 0$), parametric gain was observed, reaching CE peaks of $42.2\ dB$ at a pump power of $700\ mW$. In order to avoid gain saturation, the signal power was fixed to $1\ \mu W$. The alloy concentrations in such waveguide allowed for TPA avoidance. The structure utilised is characterised by $n_2 = 1.45 \cdot 10^{-17}\ m^2 \cdot W^{-1}$, $\gamma = 179.8\ (W \cdot m)^{-1}$, $\alpha = 57.7\ dB \cdot m^{-1}$, $L = 8.27\ cm$ and $A_{eff} = 0.33\ \mu m^2$.

4.5 Crystalline and Amorphous Silicon Waveguides

In the last section the Silicon waveguides will be examined. Silicon has widely been used in nonlinear optics [26, 27, 33, 40–43, 46–48] due to its really high nonlinearities. The crystalline and the amorphous compounds exhibit respectively $\gamma_{c-Si} \sim 21000 \times \gamma_{Silica}$ and $\gamma_{a-Si} \sim 103000 \times \gamma_{Silica}$. Such exceptionally-enhanced nonlinear coefficients have settled the Silicon devices as one remarkably promising material for the wavelength conversion. In contrast, big efforts are still intended for reducing the really high linear losses (α) displayed by the Silicon waveguides.

Moreover, one of the main drawbacks of Silicon that has emerged the interest in other media, is the notable nonlinear losses due to the TPA and the FCA phenomena. Lately, different related work have demonstrated the suppression of such free carriers by utilising either p-i-n junctions [46, 47] or slot waveguide structures [48]. The comparison has been done taking into account the 2 different schemes where only TPA influences the system and secondly, when both TPA and FCA losses reduce the efficiency.

Let us introduce the comparison by firstly presenting the analytical solution for the output power expressed in 3.12. Note that this model does not consider the absorption coming from the generated free carriers (FCA) hence, the comparison extracted from this starting analysis will not be the fairest one. Accordingly, the output power variation has been pictured versus the increase of either the length or the input power. Both comportments can be seen in Fig. 4.13.

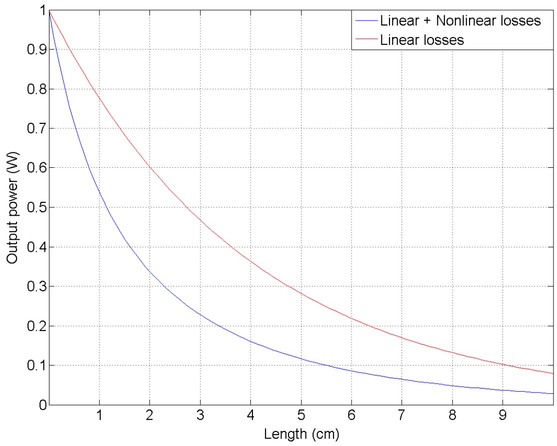

(a) P_{out} vs. length (c-Si with $P_{in} = 1\,W$).

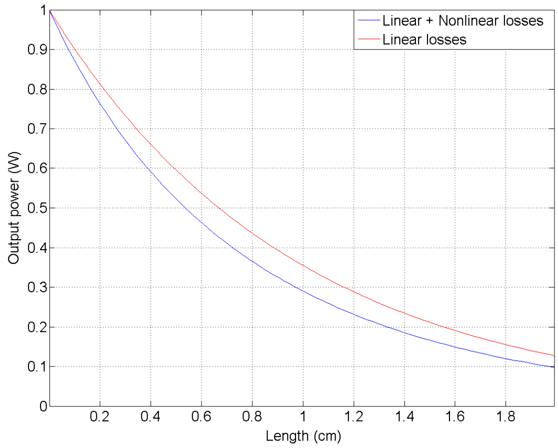

(b) P_{out} vs. length (a-Si with $P_{in} = 1\,W$).

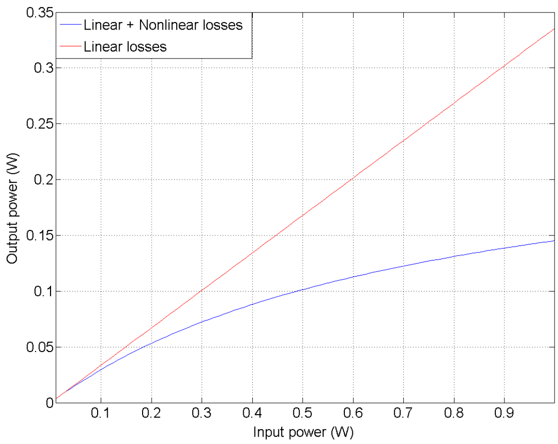

(c) P_{out} vs. P_{in} (c-Si with $L = 4.31\,cm$).

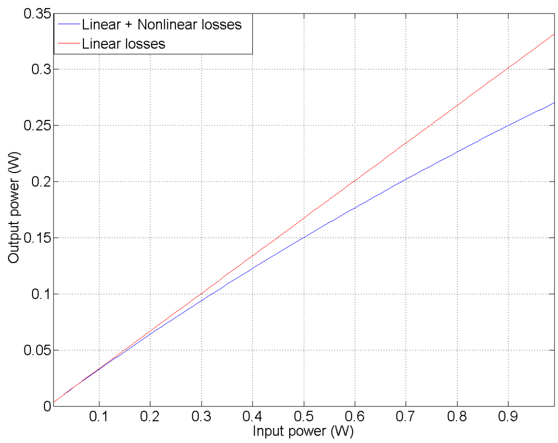

(d) P_{out} vs P_{in} (a-Si with $L = 1.06\,cm$).

Figure 4.13: Representation of the TPA analytical study showing the output power varying with (a) - (b) the length and the (c) - (d) input power for a crystalline and an amorphous Silicon waveguides, respectively. It has been compared to the linear absorption case $P_{out} = P_{in}e^{-\alpha L}$ (red line).

The increase in losses induced by TPA can be observed in both representations for the two devices. Notice that the pump power has been fixed to $1\,W$ when varying the length. Differently, in the input power sweep, the length for each device has been settled to $4.31\,cm$ and $1.06\,cm$, respectively for c-Silicon and a-Silicon, by means of linear losses minimisation ($L_{eff}^2 e^{-\alpha L}$) to be consistent in the comparison. Concurrently, an increment in length as well as in launched power give rise to higher nonlinear losses. As a consequence, the optimisation of the two parameters will be performed so as to compare these designs. This preliminary study must include, as in the previous SBS analysis, the FOM in order to stablish some benchmark. Considering both relations presented in Eq. 3.13 such factor turns out to be

$$FOM_{c-Si_1} = 2.58 \quad \longleftrightarrow \quad FOM_{a-Si_1} = 0.388$$
$$FOM_{c-Si_2} = 0.774 \quad \longleftrightarrow \quad FOM_{a-Si_2} = 5.33.$$

In one way or another, the a-Si waveguide is presenting a better FOM. In the first case presenting the lowest value, whilst taking the greater in the second definition, as requested. In addition, it will be demonstrated that a-Si devices present a better power efficiency in the wavelength conversion application.

Continuing now to the numerical evaluation, the system of coupled equations has likewise been solved for the actual devices giving the impact of TPA and FCA in the process of power minimisation. Once again, the wavelength conversion efficiency (CE) has been sought by fulfilling the maximum conditions, which is linear phase matching. The study followed in here shows the behaviours for both crystalline and amorphous Silicon structures whether TPA and FCA are affecting on the one hand, or just TPA is modifying the performance, on the other. One can observe those representations in Fig. 4.14.

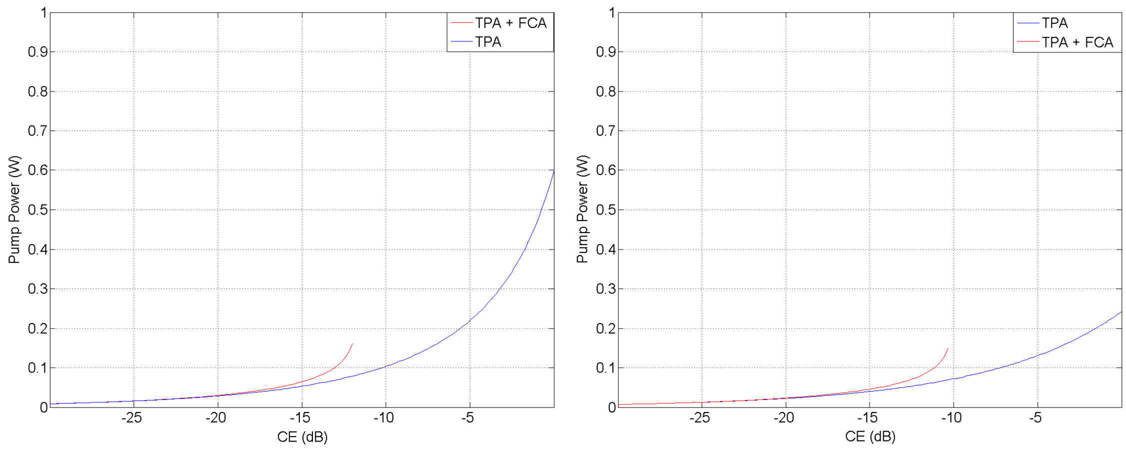

(a) Crystalline Silicon. (b) Amorphous Silicon.

Figure 4.14: Power minimisation representation. The minimum pump power required for a target CE in a (a) crystalline and an (b) amorphous Silicon waveguides.

Note that the curves containing both TPA and FCA effects are not taking values after some point. This is normal since we are looking into the minimum power requirement for a target maximum CE. These shorter curves display the fact that a better CE is not achievable hence, the minimum pump power is attained once (an extended curve would have no sense, otherwise the term "minimum power" would lose such meaning). This can be numerically clarified by an example such as

$$P_p = 161\,mW = \{min\ P_p\,|\,CE_{s-Si} = -12\,dB\}$$

hence

$$P_p = 200\,mW \implies CE_{s-Si} = -12\,dB \text{ but } P_p = 200\,mW \notin P_{min}$$

A part from that, it can be seen how the free carriers are strongly affecting the system as the power increases. In contrast, if one of the aforementioned FCA-suppression techniques

was used, the Silicon compounds would bring us quite good efficiencies. Not to mention that positive CEs would be reachable within the range of $1\ W$.
Although they are extremely lossy materials ($\alpha_{c-Si} = 110\ dB \cdot m^{-1}$ and $\alpha_{a-Si} = 450\ dB \cdot m^{-1}$), they benefit from the highest nonlinear coefficients with respect to the other compared media ($\gamma_{c-Si} = 243\ (W \cdot m)^{-1}$ and $\gamma_{a-Si} = 1200\ (W \cdot m)^{-1}$). Thereby, such high efficiencies can be reported whether no FCA is detrimentally impacting the system.

Let us lastly present another repercussion from the TPA effect. In the previous devices the optimum length has been decided in terms of linear losses (α), however, in these two materials presenting the stronger nonlinear losses, the optimum length must be reduced as the pump power increases. It is illustrated in Fig. 4.15

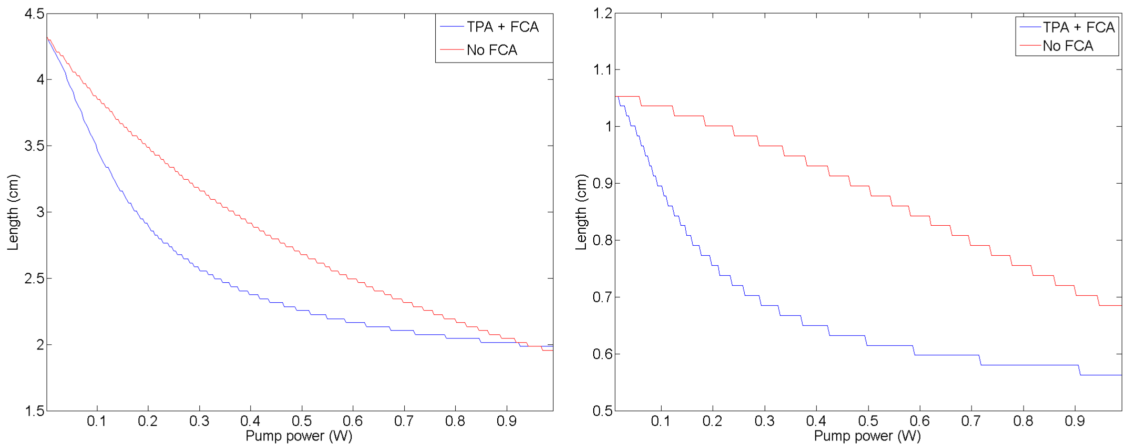

(a) Crystalline Silicon. (b) Amorphous Silicon.

Figure 4.15: Length optimisation representation. The optimum length for each pump power in a (a) crystalline and an (b) amorphous Silicon waveguides.

As optimum length it has been considered to be the one resulting in a maximum CE. Note that not a good resolution has been achieved in order to reduce the computational time for the calculations. Nonetheless, it can be seen the effect of FCA in the length reduction with the power increase. It is not methodically decreasing because FCA at high power produces power depletion thus, the CE becomes flattened and the length diminution with the power growth lose its relevance.

So far, different nonlinear media presented either in fibre or waveguide structure have been compared practically in an individual manner. The nonlinear losses coming from the scattering effect, namely stimulated Brillouin scattering (SBS), from the two-photon absorption (i.e. TPA) and from the consequently induced free-carrier absorption (FCA) have also been taken into account, showing the limiting nature they bring to the system. The scheme in all the cases has been chosen as a wavelength conversion through a degenerate four-wave mixing (DFWM).

To conclude, let us gather all the 8 selected media in one single comparison. The final result is provided in the next section.

4.6 Comparison of Selected Nonlinear Media

In this concluding section we essentially present the comparison in itself. After the introduction and analysis of these promising media in the nonlinear optics, this section is collecting the results for all of them at once. A much more clear vision will be acquired while comparing the nonlinear media all together. It is worth remarking that the results presented below have likewise been submitted in two conferences (first, to the electro-optics & communications conference CLEO-PR & OECC/PS 2013 (Kyoto, Japan) and after, to the IPC 2013 (Seattle, USA). The submitted paper can be found in the Appendix.

As the analytical methods are neither giving an accurate interpretation nor a fair comparison between fibres and waveguides, the numerical model described by [33] has been adopted. Relying on the coupled equations to solve the fields propagation and therefore, calculate the CE, the individually afore-presented behaviours have been assembled all together. The resulting comparison is pictured in Fig. 4.16.

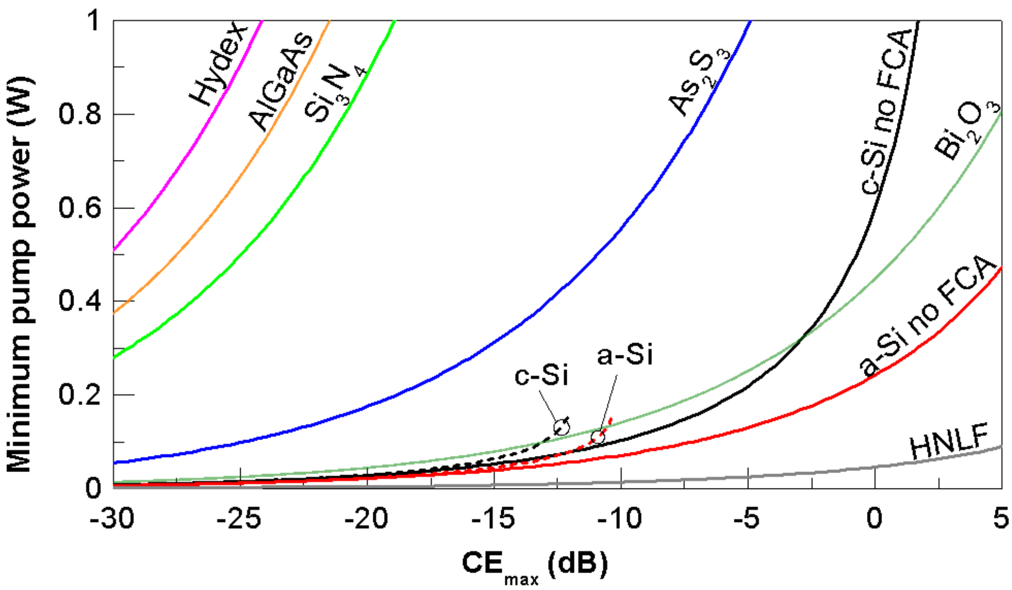

Figure 4.16: Power minimisation representation. The minimum pump power required for a target CE in all the nonlinear media presented before.

As a reminder, all the compared media in this thesis has been elected from the literature review trying to find the best and more recently manufactured devices. It is worth commenting that usually the media presenting the lowest possible linear losses (α) while exhibiting enhanced Kerr nonlinearities (γ) have been sought. Indeed, some of the media still are under investigation to achieve better performances however, not a fully-described

and already-tested example has been found in the research.
As aforementioned, for instance, III-V semiconductors (i.e. AlGaAs in the present case) show encouraging theoretical behaviours. Equally, FCA in Silicon devices has lately been reduced by using some techniques which brings us really good performances. In the case of Chalcogenide glasses, whether both the SBS (in the fibres) and the TPA (in the waveguides) phenomena could be avoided, good efficiencies are obtained. Furthermore, some recent studies suggested optimistic devices [35, 49].
Regarding the widely used Silica HNLFs, they allow for extremely high efficiencies but not for short devices in the CE maximisation. Some novel work has been intended for improving the dispersion instabilities along the fibre [50–52]. In the present work neither dispersion effects nor polarisation changes have been accounted for.

Additionally, the comparison for the optimum length of such devices has depicted in order to provide a much more clear idea for the structures design. Notice that great importance has been destined to the power optimisation though, the manufacturing of these up-to-date devices is also important. Henceforth, the different lengths variation with the pump power are pictured in Fig. 4.17.

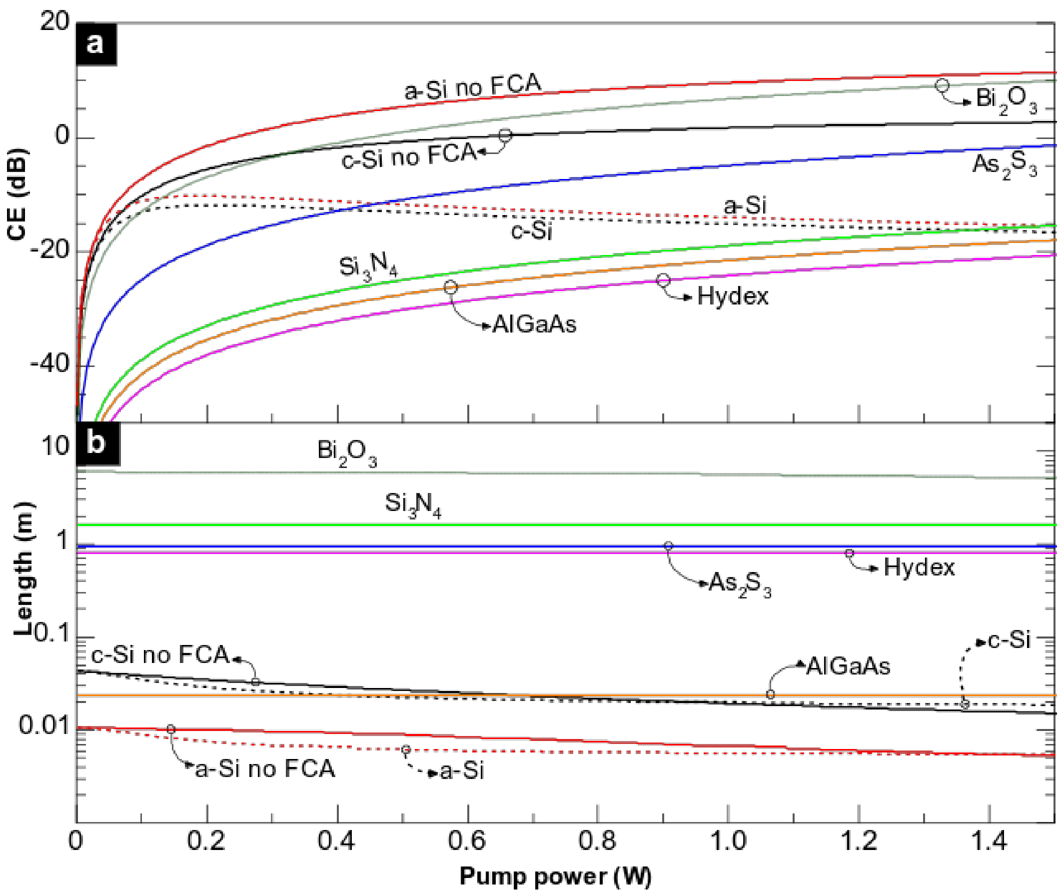

Figure 4.17: Graphical representation of the (a) Conversion Efficiency and (b) optimum length with the input pump power increase for all the nonlinear media presented before. Note that the lower plot is represented in log scale to improve the clarity between all the curves.

It is worth observing that no power minimisation is considered in Fig. 4.17. The graphic is showing the optimisation of the length with an increase of the pump power concerning, always, about the maximum CE. The latter has additionally been pictured (a) to provide a better understanding of the optimisation procedure for such length. All the points depicted in this CE curve result from the corresponding couple $[P_p, L_{opt}]$, whose relation is delineated in (b). Notice that Silica HNLF has been deleted from this group-comparison since the optimum length was about $6\,km$, which is much lengthier than the rest of devices, distorting then the clearness of this graph.

To sum up, one could assert that the Silica HNLFs bring us the best performance in terms of CE maximisation at the price however, of very long devices. Similarly, Bismuth-oxide HNLF reaches a really high efficiency while allowing for quite short devices within the range of $1\,W$.
On the other hand, regarding the waveguide structures, it can be split into three different groups. Firstly, Hydex®, AlGaAs and Silicon Nitride present results on CE in between $-25\,dB$ and $-20\,dB$ for power minimisation, being the Si_3N_4 the one with the higher CE. Optimising the length, Silicon Nitride result in designs of almost $2\,m$, Hydex® in lengths close to $1\,m$ and the III-V semiconductor (AlGaAs) allows for the shorter device which is about $2\,cm$.
Secondly, the Chalcogenide (As_2S_3) waveguide shows a quite good CE, almost achieving positive values, with an optimum device length of $1\,m$. As stated before, some promising designs may provide higher efficiencies. We must recall that high powers are not recommended in such media.
Finally, the third group consists of the Silicon compounds (both crystalline and amorphous). It has been shown that such devices exhibit strong drawbacks coming from TPA and FCA. Nonetheless, some techniques can avoid them shifting the CE for such media from $[-12, -10]\ dB$ up to positive values. One could observe an enhancement in the a-Si case, since the maximum attainable CE saturates at higher powers. Besides, these two mediums permit the shortest optimum devices. Note that the length variation in these cases is important whether the power keeps incrementing. Crystalline Silicon optimum designs must be shorter than $4\,cm$ while amorphous Silicon devices cannot exceed lengths of $1\,cm$.
Hence, only those materials reaching at least $CE = 0dB$, which are (from the results) Silica and Bismuth HNLFs and, the amorphous and crystalline Silicon (a-Si and c-Si, respectively) waveguides when no FCA is affecting, allow for the avoidance of an extra-amplifier box adding noise to the signal.

CHAPTER 5

Conclusions and Future Work

This Master Thesis has been focused on the comparison between different nonlinear media widely used in various studies regarding the CE (and so, the amplification) of a transmitted signal.
The case-study proposed in here, as in many other cases found in the literature review, consist of a degenerate FWM scheme. The effects of the different selected nonlinear media on the resulting output wave (idler) has been examined both analytically and numerically. The latter method has been realised by means of Matlab® tool.

After a thorough research concerning up-to-the-minute nonlinear media, different effects emerging from such materials peculiarities have been described such as SHG, SFG and DFG as $\chi^{(2)}$ nonlinearities, and from the other hand, Kerr effects, FWM, TPA and SBS as $\chi^{(3)}$ nonlinearities. Either the frequency (wavelength) conversion process or the efficiency reducer phenomena (SBS, TPA and FCA) have been useful in the comparison.

Furthermore, all the investigation tools together with the comparison procedure used in this work have been described. Accordingly, results on the TPA, FCA and SBS have been presented in order to provide a benchmark for these nonlinear media. In addition, the consequent CE for each media has been detailed as well.
Divided into two main groups one can find the study of the HNLFs made of either Silica (SiO_2) or Bismuth-Oxide (Bi_2O_3) and, by contrast, the second group, which consists of Hydex®, Si_3N_4, $AlGaAs$, As_2S_3, crystalline and amorphous Silicon, includes the waveguides analyses.

SBS evidences have been demonstrated in the fibres examination. In both cases, SiO_2 and Bi_2O_3, the commonly named SBST has been investigated. Firstly, in an analytical method and after, for a more precise estimation, numerically, obtaining (by means of the latter method) values of $P_{th_{Silica}} = 11.1\ dBm$ and $P_{th_{Bismuth}} = 25.7\ dBm$.

Despite no SBS symptoms are present in the waveguide structures, some of them exhibit power efficiency reduction owing to the effects of either TPA or FCA. Similarly, analytical results (showing some FOM for the TPA comparison) have been provided together with the numerical examination for the TPA and the FCA effects on the CE.

Regarding the main scope of this work, the comparison between all the elected media has been accomplished by power and length optimisation. Thanks to the numerical investigation by means of the set of coupled equations, the materials collection has been outlined in two different graphs. On the one hand, it can be seen the minimum power required to achieve a certain maximum CE. On the other hand, an alternative design comparison has been presented by illustrating the optimum length required for each device while varying the pump power.

The materials determination has been effectuated based on the lowest linear losses (α). Accordingly, the comparison provide us with a general view gathering different nonlinear media utilised for wavelength conversion applications. More precisely, this study has been focused on the CE concerning the idler signal generated at the output as a result of the wave mixing (DFWM) from the input signals. Such efficiency parameter gives us an amplification knowledge on the nonlinear materials. As a consequence, it can be seen that a few media allow for keep the system away from using extra-amplifier boxes, which results in no extra-noise addition to the performance. At the present comparison, amplification (within the range of $1\ W$) has been observed in both fibres (Silica and Bismuth-oxide) together with the waveguides made of crystalline and amorphous Silicon when FCA is eradicated. However, some advanced studies are presenting amplification in Chalcogenide and $AlGaAs$ devices.

As aforementioned, neither dispersion nor polarization effects have been considered in this comparison. Hence, the values obtained in the comparison would be slightly downshifted in terms of CE, since these effects would entail efficiency reduction basically in the fibres analyses. As one could see, the optimum length for the Silica fibre is about $6\ km$, which is much longer than the ones normally used in practice ($300 - 500\ m$). Thus, such effects would have an important impact on the CE, since the perfect linear phase mismatch assumption ($\Delta\beta = 0$) would be no longer acceptable. Therefore, such imperfections inclusion together with a practical examination in the laboratory should be implemented in the next future to get a much more accurate comparison. Moreover, considering the noise addition by a well-known amplifier, a Bit Error Rate (BER) comparison could be included for the media that need such amplifier. Finally, other up-and-coming nonlinear materials could be investigated to increase the benchmark carried out herein to help the designer out choosing the appropriate device for wavelength conversion applications.

Appendices

APPENDIX **A**

Basic Concepts

A.1 Maxwell Equations

Similar to many fields in the Physics, the study of the propagation of the optical fields branch emerge from the well-known Maxwell Equations. They are used to obtain the wave equation describing the light propagations along the devices. Such equations in the SI (International System) units are given by [1]

$$\bigtriangledown \times \mathbf{E} = -\frac{\delta \mathbf{B}}{\delta t}, \tag{A.1a}$$

$$\bigtriangledown \times \mathbf{H} = \mathbf{J} + \frac{\delta \mathbf{D}}{\delta t}, \tag{A.1b}$$

$$\bigtriangledown \cdot \mathbf{D} = \rho, \tag{A.1c}$$

$$\bigtriangledown \cdot \mathbf{B} = 0, \tag{A.1d}$$

where $\mathbf{E}$ and $\mathbf{H}$ are electric and magnetic field vectors, respectively, and $\mathbf{D}$ and $\mathbf{B}$ are corresponding electric and magnetic flux densities described as

$$\mathbf{D} = \varepsilon_0 \mathbf{E} + \mathbf{P}, \tag{A.2a}$$

$$\mathbf{B} = \mu_0 \mathbf{H} + \mathbf{M}, \tag{A.2b}$$

where $\mathbf{P}$ and $\mathbf{M}$ are the induced electric and magnetic polarizations, respectively, and ε_0 and μ_0 are the vacuum permittivity and permeability.
In absence of free charges and considering non-magnetic media the following approximations are considered

$$\rho = 0, \qquad \mathbf{J} = 0, \qquad \mathbf{M} = 0\ (\mathbf{B} = \mu_0 \mathbf{H}). \tag{A.3}$$

A.2 Frequency and Wavelength Relations

The main topic in this thesis has been the CE regarding the efficiency in the wavelength (or frequency) conversion process. Both the frequency, f, and the wavelength, λ, domains are directly related by

$$f\ [Hz] = \frac{c}{\lambda} \quad \Longrightarrow \quad \omega_1 + \omega_2 = \omega_3 \ \equiv \ \frac{1}{\lambda_1} + \frac{1}{\lambda_2} = \frac{1}{\lambda_3}, \tag{A.4a}$$

$$\Delta f = \frac{c}{\lambda^2}\Delta\lambda \quad (Bandwidth\ relationship)\,. \tag{A.4b}$$

A.3 Linear Losses

The main detrimental effect present in this devices are the linear losses. Throughout many years, big efforts have been intended for reducing such effect in these nonlinear devices. Such losses become gathered in the so-called attenuation parameter, α, that describes the power-reduction through

$$\frac{\delta P(z)}{\delta z} = -\alpha z \quad \Longrightarrow \quad P(z) = P_0 e^{-\alpha z}. \tag{A.5}$$

The attenuations is usually expressed in $\left[\frac{dB}{km}\right]$ or $\left[\frac{dB}{cm}\right]$ when the material presents really high losses and hence, short devices are employed. Such phenomena depends on the wavelength range the device is used. The following picture reflects this frequency dependence for a Silica fibre A.1.

All the simulations along the thesis have been made under the $\lambda = 1550\,nm$ window which can be seen is the lowest losses range. Outstanding optical fibres already reached values around $0.2\,\frac{dB}{km}$. However, due to the required highly nonlinear characteristics, such losses are quite higher in the materials studied in this document.

Besides, this linear losses determine the effective length of the device defined as follows

$$L_{eff} = \frac{1 - e^{-\alpha L}}{\alpha}, \tag{A.6}$$

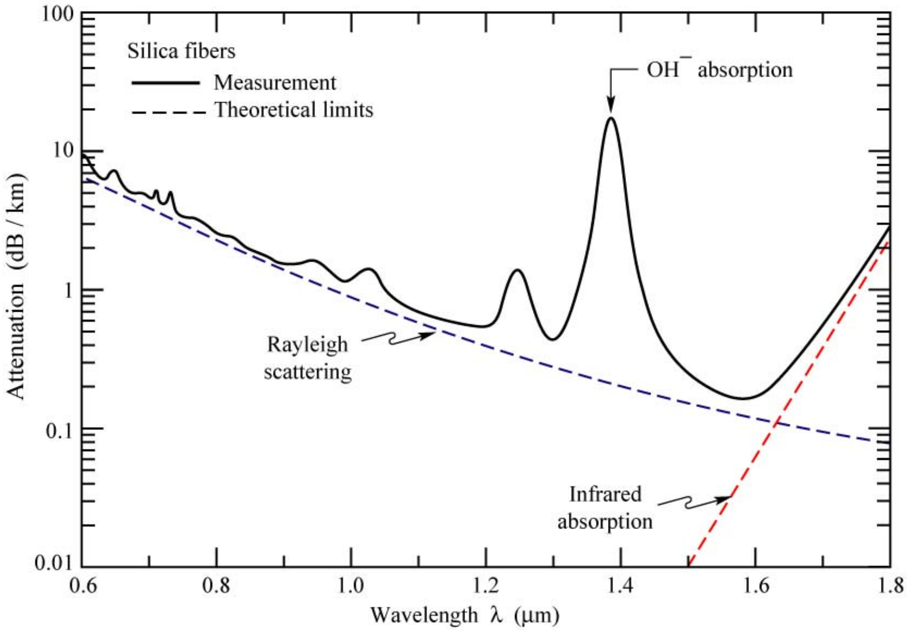

Figure A.1: Attenuation spectrum for a Silica fibre. Picture extracted from www.lightemittingdiodes.org.

where L stands for the physical length of the device.

Another typical parameter taken into consideration in nonlinear effects calculations is the effective mode area, A_{eff}, which is expressed by

$$A_{eff} = \frac{\left(\iint_{-\infty}^{\infty} |F(x,y)|^2 dxdy\right)^2}{\iint_{-\infty}^{\infty} |F(x,y)|^4 dxdy}, \tag{A.7}$$

where $F(x,y)$ is the modal distribution of the device.

APPENDIX **B**

Article Submitted

B.1 Paper Submission

In this second appendix we present the paper regarding the thesis main topic submitted in both the electro-optics & communications conference CLEO-PR & OECC/PS 2013 (Kyoto, Japan) and after, to the IPC 2013 (Seattle, USA). Although it was rejected in the first attempt (CLEO-PR & OECC/PS), the article has been accepted for the upcoming conference that will be held in Seattle (IPC 2013).

A Comparison of Nonlinear Media for Parametric All-Optical Signal Processing

Jordi Martínez Díaz, Jaume Bohigas Nadal, Dragana Vukovic, Francesco Da Ros, Evarist Palushani, and Christophe Peucheret*
Department of Photonics Engineering, Technical University of Denmark. DK-2800 Kgs. Lyngby, Denmark
*cpeu@fotonik.dtu.dk

Abstract

We systematically compare nonlinear media for parametric signal processing by determining the minimum pump power that is required for a given conversion efficiency in a degenerate four-wave mixing process, including the effect of nonlinear loss.

I. Introduction

All-optical signal processing relies on nonlinear media through which optical waves are made to interact. Among the available physical mechanisms, third order parametric processes are particularly attractive since they allow the realization of a wide range of functionalities, including wavelength conversion, phase conjugation, switching, sampling, logic and amplification. Traditionally, specially designed highly nonlinear fibers (HNLFs) have been largely used for the demonstration of parametric signal processing [1]. In spite of their low loss and inherent compatibility with fiber optic systems, they are however limited by a relatively modest Kerr nonlinearity.

Recently, a wealth of alternative media presenting enhanced Kerr nonlinearity, sometimes several orders of magnitude large than that of HNLFs, have emerged. Those include, among others, bismuth oxide fibers [2], as well as waveguides (WGs) made of cristalline [3] or amorphous [4,5] silicon, silicon nitride [6], chalcogenide glass [7], AlGaAs [8] or high-index doped silica glass (Hydex®) [9]. The motivation behind the introduction of these material is not only to obtain higher nonlinear coefficients thanks to their enhanced nonlinear index and strong confinement, but also the possibility of dispersion engineering enabling phase matching over a wide bandwidth. However, in spite of their attractive Kerr nonlinearity, these materials may also suffer from drawbacks including linear and nonlinear loss or stimulated Brillouin scattering (SBS), which limit the achievable conversion efficiency. Although extensive literature demonstrates applications of these materials individually, their relative merits are so far unclear.

In this paper, we report a thorough and systematic comparison of nonlinear media for parametric signal processing. By estimating the pump power required in a degenerate pump wavelength conversion process, we highlight the relative strengths and weaknesses of eight popular nonlinear media.

II. Description of the Model

The study focuses on the estimation of the maximum attainable conversion efficiency (CE, defined as the ratio of the idler power at the waveguide output to the signal power at its input) in a degenerate four-wave mixing (FWM) wavelength conversion process. For this purpose the system of equations linking the complex envelopes of the signal A_s, the pump A_p and the idler A_i is solved under continuous wave (CW) operation,

$$\frac{dA_p}{dz} = -\frac{1}{2}\left(\alpha + \alpha_{TPA,p} + \alpha_{FCA}\right)A_p + j\gamma\left(\left|A_p\right|^2 + 2\left|A_s\right|^2 + 2\left|A_i\right|^2\right)A_p + 2j\gamma A_p^* A_s A_i e^{j\Delta\beta z},$$

$$\frac{dA_{s,i}}{dz} = -\frac{1}{2}\left(\alpha + \alpha_{TPA s,i} + \alpha_{FCA}\right)A_{s,i} + j\gamma\left(\left|A_{s,i}\right|^2 + 2\left|A_p\right|^2 + 2\left|A_{i,s}\right|^2\right)A_{s,i} + j\gamma A_{i,s}^* A_p^2 e^{-j\Delta\beta z}.$$

α is the linear loss, γ is the nonlinear (Kerr) coefficient and $\Delta\beta$ is the linear phase mismatch between the waves. The nonlinear loss due to two-photon absorption (TPA) and TPA-induced free-carrier absorption (FCA) are

$$\alpha_{TPA,k} = \frac{\beta_{TPA}}{A_{eff}}\left(\left|A_k\right|^2 + 2\sum_{m\neq k}\left|A_m\right|^2\right),$$

$$\alpha_{FCA} = \frac{\sigma\beta_{TPA}\tau_c}{2hcA_{eff}^2}\left(\sum_m \lambda_m\left|A_m\right|^4 + 4\sum_{m\neq n}\frac{\lambda_m\lambda_n\left|A_m\right|^2\left|A_n\right|^2}{\lambda_m+\lambda_n}\right),$$

respectively. β_{TPA} is the TPA coefficient, σ_{FCA} is the FCA cross-section, A_{eff} is the effective area and τ_c is the carrier lifetime. This model is valid in the absence of pump depletion by the FWM process. In case of SBS, the threshold is defined as the value of the input pump power for which 1% of the power is back-scattered and is calculated using a shooting algorithm. The maximum CE is obtained under phase matching condition $\Delta\beta$=0 at a pump wavelength of 1550 nm. The comparison is performed between the nonlinear materials in Table I.

III. Results and Discussion

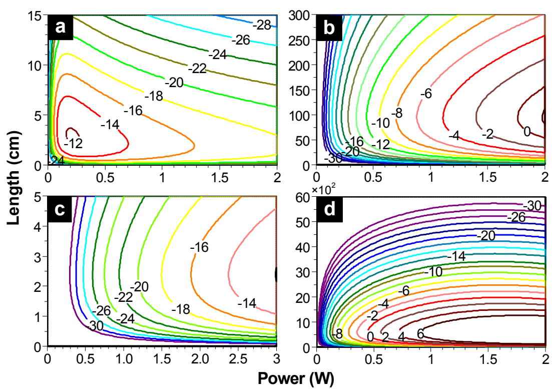

Fig. 1. CE as a function of waveguide length and pump power for (a) crystalline silicon (c-Si), (b) chalcogenide (As_2S_3), (c) $Al_{0.18}Ga_{0.82}As$ waveguides and (d) bismuth oxide (Bi_2O_3) fiber.

TABLE I
NONLINEAR MATERIALS PARAMETERS

	γ	α	A_{eff}	β_{TPA}	σ_{FCA}	τ_c	g_B	Ref
	($W^{-1}{\cdot}m^{-1}$)	($dB{\cdot}cm^{-1}$)	(μm^2)	($cm{\cdot}GW^{-1}$)	(m^2)	(ns)	($m{\cdot}W^{-1}$)	
silica HNLF	11.5×10^{-3}	8×10^{-6}	11	-	-	-	7.9×10^{-12}	[1]
Bi_2O_3 HNLF	1.1	8×10^{-3}	3	-	-	-	6.4×10^{-11}	[2]
c-Si WG	2.43×10^{2}	1.1	0.1	0.5	1.45×10^{-21}	1	-	[3,10]
a-Si WG	1.2×10^{3}	4.5	0.07	0.25	1.9×10^{-20}	0.4	-	[4,5]
Si_3N_4 WG	0.2	3×10^{-2}	1.8	-	-	-	-	[6]
As_2S_3 WG	1.7	5×10^{-2}	6.9	6×10^{-4}	-	-	-	[7]
AlGaAs WG	10	2	5.7	0.05	-	-	-	[8]
High index silica WG	0.22	6×10^{-2}	2	-	-	-	-	[9]

First, the CE is calculated as a function of waveguide or fiber length and pump power, as illustrated for sample materials in Fig. 1. This enables to determine the optimum length that minimizes the pump power for a given value of CE. For materials presenting nonlinear absorption, such as silicon, the optimum length depends on the pump power. In case of materials presenting only linear loss, it corresponds to the value obtained from maximizing $L_{eff}e^{-\alpha L}$, where $L_{eff}=(1-e^{-\alpha L})/\alpha$ is the effective length. The minimum pump powers resulting in a given maximum CE (i.e. at phase matching) are represented in Fig. 2. This minimum required pump power ($P_{p,min}$) is considered to be a good figure of merit to compare the intrinsic benefits of the materials since it assess the pump power efficiency of the process for the same functional performance.

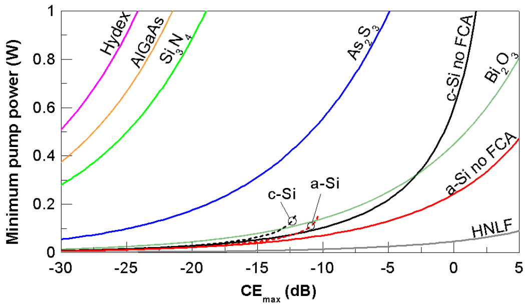

Fig. 2. Minimum pump power required to achieve a given CE for the different materials.

The results of Fig. 2 are limited to the regime where no strong parametric gain is achieved, and where the undepleted pump approximation is valid. Parametric gain could be obtained at higher pump powers for some of the media, for instance silica HNLF. However, this would require SBS mitigation techniques to be implemented, which is outside the scope of the study. Based on our SBS threshold definition, the pump power should be limited in practice to 1 mW for silica HNLF and 390 mW for Bi_2O_3 HNLF (at the optimum fiber lengths of 5.8 km and 6 m, respectively) if no SBS countermeasure is used. For Si, in which carriers are generated via TPA, $P_{p,min}$ has also been calculated neglecting FCA, which would constitute an optimum case when the generated carriers are removed using a reverse-biased p-i-n junction.

Among the investigated media, silica HNLFs allow to achieve a given CE for the smallest pump power thanks to their low loss allowing long interaction length. Note that the calculations assume perfect phase matching, which would be challenging in practice for long HNLFs. The linear losses of high index silica (Hydex®), silicon nitride (Si_3N_4) and chalcogenide (As_2S_3) waveguides are of the same order of magnitude, but the former two media are limited by their smaller γ. Their performance is similar to that of $Al_{0.18}Ga_{0.82}As$, which presents higher linear loss but a larger γ. Crystalline (c-Si) and amorphous (a-Si) silicon benefit from their high γ but are limited to CEs to about -10 dB due to TPA and FCA. If FCA can be suppressed, a-Si offers the second best performance after silica HNLFs. The performance of bismuth oxide (Bi_2O_3) nearly matches that of c-Si (without FCA) until it reaches its SBS threshold.

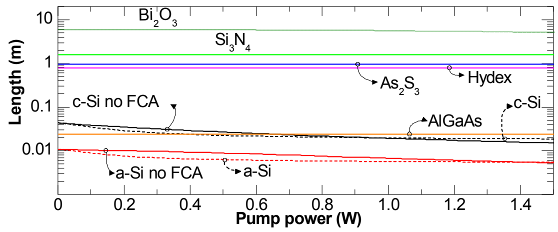

Fig. 3. Optimum waveguide lengths at which the minimum pump powers in Fig. 2 are obtained.

The waveguide lengths corresponding to the maximum reachable CEs are also shown in Fig. 3 for the planar waveguide materials. It is clear that if TPA and FCA are present, the waveguide length needs to be optimized for each pump power.

IV. CONCLUSIONS

We have performed a systematic comparison of nonlinear media for all-optical signal processing in case of degenerate FWM wavelength conversion. The relative impact of loss (linear and nonlinear) and nonlinear coefficient has been assessed for a fixed CE target.

REFERENCES

[1] D.J. Richardson et al., ECOC (2010) Tu.4.D.1.
[2] J. H. Lee et al. Opt. Lett. 30, (2005) 1698-1700.
[3] M. A. Foster et al. Nature 441 (2006) 960-963.
[4] C. Grillet et al., Opt. Express 20, (2012) 22609–22615.
[5] K. Narayanan and S. F. Preble, Opt. Express 18 (2010) 8998–9005..
[6] M.-C. Tien et al., Opt. Express 18 (2010) 23562-23568.
[7] B. J. Eggleton et al., Nature Photon. 5 (2011) 141-148.
[8] K. Dolgaleva et al., Opt. Express 19 (2011) 12440-12455.
[9] D. Duchesne et al., Opt. Express 17 (2009) 1865-1870.
[10] Q. Lin et al., Opt. Express, 15 (2007) 16604-16644.

Bibliography

[1] Govind P. Agrawal. *Nonlinear Optics*. Academic Press, 2006.

[2] Robert Boyd. *Nonlinear Optics*. Academic Press, 2008.

[3] Bahaa E. A. Saleh and Malvin Carl Teich. *Fundamentals of Photonics*. John Wiley and Sons, 2007.

[4] Rüdiger Paschotta. Rp photonics consulting gmbh. *http://www.rp-photonics.com*.

[5] Lucia Caspani, David Duchesne, Ksenia Dolgaleva, Sean J. Wagner, Marcello Ferrera, Luca Razzari, Alessia Pasquazi, Marco Peccianti, David J. Moss, J. Stewart Aitchison, and Roberto Morandotti. Optical frequency conversion in integrated devices. *Optical Society of America*, 28(12), 2011.

[6] W. Kaiser and C. G. B.Garrett. Two-photon excitation in Ca F_2:Eu^{2+}. *Physical Review Letters*, 7(6), 1961.

[7] Alex Hayat, Amir Nevet, Pavel Ginzburg, and Meir Orenstein. Applications of two-photon processes in semiconductor photonic devices. *Semiconductor Science and Technology*, 26, 2011.

[8] R. Y. Chiao, C. H. Townes, and B. P. Stoicheff. Stimulated brillouin scattering and coherent generation of intense hypersonic waves. *Physical Review Letters*, 12(21), 1964.

[9] S. P. Singh, R. Gangwar, and N. Singh. Nonlinear scattering effects in optical fibers. *Progress In Electromagnetics Research*, 74:379 – 405, 2007.

[10] Andrey Kobyakov, Michael Sauer, and Dipak Chowdhury. Stimulated Brillouin scattering in optical fibers. *Advances in Optics and Photonics*, 2:1 – 59, 2010.

[11] K. S. Abedin. Efficient Stokes Wave Generation by Brillouin Scattering in Single-Mode Chalcogenide Fiber. *Optical Society of America*, 2006.

[12] Guanshi Qin, Hideyuki Sotobayashi, Masahiro Tsuchiya, Atsushi Mori, Takenobu Suzuki, and Yasutake Ohishi. Stimulated Brillouin Scattering in a Single-Mode Tellurite Fiber for Amplification, Lasing, and Slow Light Generation. *Journal of Lightwave Technology*, 26(5), 2008.

[13] Robert W. Boyd. Material slow light and strutural slow light: similarities and differences for nonlinear optics. *Optical Society of America*, 28(12), 2011.

[14] Christophe Peucheret. Note on impact of slow light on fwm conversion efficiency. 2012.

[15] C. Monat, M. de Sterke, and B. J. Eggleton. Slow light enhanced nonlinear optics in periodic structures. *Journal of Optics*, 12, 2010.

[16] Lars Grüner-Nielsen, Søren Herstrøm, Sonali Dasgupta, David Richardson, Dan Jakobsen, Carl Lundström, Peter A. Andrekson, Martin E. V. Pedersen, and Bera Pálsdóttir. Silica-Based Highly Nonlinear Fibers with a High SBS Threshold. *Winter Tropicals (WTM), IEEE*, 2011.

[17] P. Bayvel and P. M. Radmore. Solutions of the SBS Equations in Single Mode Optical Fibres and Implications for Fibre Transmission Systems. *Electronics Letters*, 26(7), 1990.

[18] A. Djupsjöbacka, G. Jacobsen, and B. Tromborg. Dynamic Stimulated Brillouin Scattering Analysis. *Journal of Lightwave Technology*, 18(3), 2000.

[19] Kazi S. Abedin. Efficient Slow Light Generation Using Highly Nonlinear Non-Silica-Based Fibers. *We.B4.4, International Conference on Transparent Optical Networks (ICTON)*, 2007.

[20] Ju Han Lee, Takuo Tanemura, Kazuro Kikuchi, Tatsuo Nagashima, Tomoharu Hasegawa, Seiki Ohara, and Naoki Sugimoto. Experimental comparison of a Kerr nonlinearity figure of merit including the stimulated Brillouin scattering threshold for state-of-the-art nonlinear optical fibers. *Optics Letters (OSA)*, 30(13), 2005.

[21] Francesco Da Ros. Multilevel Signal Processing Using Phase Sensitive Amplification. Master's thesis, Technical Universtity of Denmark (DTU), 2011.

[22] Victor Mizrahi, K. W. DeLong, G. I. Stegeman, M. A. Saifi, and M. J. Andrejco. Two-photon absorption as a limitation to all-optical switching. *Optics Letters (OSA)*, 14(20), 1989.

[23] Masaki Asobe. Nonlinear Optical Properties of Chalcogenide Glass Fibers and Their Application to All-Optical Switching. *Optical Fiber Technology*, 3(OF970214):142 – 148, 1997.

[24] H. C. Nguyen, K. Finsterbusch, D.J. Moss, and B. J. Eggleton. Dispersion in nonlinear figure of merit of As_2Se_3 chalcogenide fibre. *Electronics Letters*, 42(10), 2006.

[25] Mariacristina Rumi and Joseph W. Perry. Two-photon absorption: an overview of measurements and principles. *Advances in Optics and Photonics*, 2:451 – 518, 2010.

[26] Karthik Narayanan and Stefan F. Preble. Optical nonlinearities in hydrogenated-amorphous silicon waveguides. *Optics Express*, 18(9), 2010.

[27] P. Mehta, N. Healy, R. Slavík, R. T. Watts, J. R. Sparks, T. D. Day, P. J. A. Sazio, J. V. Badding, and A. C. Peacock. Nonlinearities in Silicon Optical Fibers. *OSA/OFC/NFOEC*, 2011.

[28] Gian-Mattia Schucan, Radu G. Ispasoiu, A. Mark Fox, and John F. Ryan. Ultrafast Two-Photon Nonlinearities in CdSe Near 1.5 μm Studied by Interferometric Autocorrelation. *IEEE Journal of Quantum Electronics*, 34(8), 1998.

[29] Masaki Asobe, Terutoshi Kanamori, Kazunori Naganuma, Hiroki Itoh, and Toshikuni Kaino. Thirdorder nonlinear spectroscopy in As_2S_3 chalcogenide glass fibers. *Journal of Applied Physics*, 77(11), 1995.

[30] L. B. Fu, M. Rochette, V. G. Ta'eed, D. J. Moss, and B. J. Eggleton. Investigation of self-phase modulation based optical regeneration in single mode As_2Se_3 chalcogenide glass fiber. *Optics Express*, 13(19), 2005.

[31] Nori Shibata, Ralf P. Braun, and Robert G. Waarts. Phase-Mismatch Dependence of Efficiency of Wave Generation Through Four-Wave Mixing in a Single-Mode Optical Fiber. *IEEE Journal of Quantum Electronics*, 23(7), 1987.

[32] Roger H. Stolen and John E. Bjorkholm. Parametric Amplification and Frequency Conversion in Optical Fibers. *IEEE Journal of Quantum Electronics*, 18(7), 1982.

[33] Shiming Gao and Sailing He. *Nanowires - Fundamental Research*, chapter 2: Four-Wave Mixing in Silicon Nanowire Waveguides and Its Applications in Wavelength Conversion. InTech, 2011.

[34] D. J. Richardson, X. Feng, F. Poletti, S. Dasgupta, A. Camerlingo, F. Parmigiani, P. Petropoulos, W. H. Loh, Søren Herstrøm, and Lars Grüner-Nielsen. Recent Advances in Highly Nonlinear Fibres. *IEEE ECOC Tu.4.D.1*, 2010.

[35] Benjamin J. Eggleton, Barry Luther-Davies, and Kathleen Richardson. Chalcogenide photonics. *Nature Photonics*, 5, 2011.

[36] X. Feng, G. M. Ponzo, F. Poletti, A. Camerlingo, F. Parmigiani, M. N. Petrovich, P. Petropoulos, N. M. White, W. H. Loh, and D. J. Richardson. A Single-mode, High Index-contrast, Lead Silicate Glass Fibre with High Nonlinearity, Broadband

Near-zero Dispersion at Telecommunication Wavelengths. *IEEE ECOC Tu.4.D.2*, 2010.

[37] Ksenia Dolgaleva, Wing Chau Ng, Li Qian, and J. Stewart Aitchison. Compact highly-nonlinear AlGaAs waveguides for efficient wavelength conversion. *Optics Express*, 19(13), 2011.

[38] David Duchesne, Marcello Ferrera, Luca Razzari, Roberto Morandotti, Brent E. Little, Sai T. Chu, and David J. Moss. Efficient self-phase modulation in low loss, high index doped silica glass integrated waveguides. *Optics Express*, 17(3), 2009.

[39] Ming-Chun Tien, Jared F. Bauters, Martijn J. R. Heck, Daniel J. Blumenthal, and John E. Bowers. Ultra-low loss Si_3N_4 waveguides with low nonlinearity and high power handling capability. *Optics Express*, 18(23), 2010.

[40] Mark A. Foster, Amy C. Turner, Jay E. Sharping, Bradley S. Schmidt, Michal Lipson, and Alexander L. Gaeta. Broad-band optical parametric gain on a silicon photonic chip. *Nature*, 441, 2006.

[41] Q. Lin, Oskar J. Painter, and Govind P. Agrawal. Nonlinear optical phenomena in silicon waveguides: Modeling and applications. *Optics Express*, 15(25), 2007.

[42] C. Grillet, L. Carletti, C. Monat, P. Grosse, B. Ben Bakir, S. Menezo, J. M. Fedeli, and D. J. Moss. Amorphous silicon nanowires combining high nonlinearity, FOM and optical stability. *Optics Express*, 20(20), 2012.

[43] Karthik Narayanan and Stefan F. Preble. Optical nonlinearities in hydrogenated-amorphous silicon waveguides. *Optics Express*, 18(9), 2010.

[44] Masaaki Hirano, Tetsuya Nakanishi, Toshiaki Okuno, and Masashi Onishi. Silica-Based Highly Nonlinear Fibers and Their Application. *IEEE Journal of Selected Topics in Quantum Electronics*, 15(1), 2009.

[45] Jaume Bohigas. Optimisation of parametric processes in nonlinear optical waveguides. Master's thesis, Technical Universtity of Denmark (DTU), 2013.

[46] A. Gajda, G. Winzer, B. Tillack, K. Petermann, L. Zimmermann, and H. Tian. High Efficiency CW Four-Wave Mixing at $1.5\ \mu m$ in SOI Nano-Rib Waveguides Using p-i-n Diodes. *ThD7, IEEE*, 2012.

[47] Andrzej Gajda, Lars Zimmermann, Mahmoud Jazayerifar, Georg Winzer, Hui Tian, Robert Elschner, Thomas Richter, Colja Schubert, Bernd Tillack, and Klaus Petermann. Highly efficient CW parametric conversion at 1550 nm in soi waveguides by reverse biased p-i-n junction. *Optics Express*, 20(12), 2012.

[48] T. Vallaitis, C. Koos, B. Esembeson, I. Biaggio, T. Michinobu, F. Diederich, P. Dumon, R. Baets, W. Freude, and J. Leuthold. Highly Nonlinear Silicon Photonics Slot Waveguides without Free Carrier Absorption Related Speed-Limitations. *IEEE ECOC Th.2.D.6*, 4, 2008.

[49] Duk-Yong Choi, Xin Gai, Steve Madden, Rongping Wang, and Barry Luther-Davies. Silver-doped Arsenic Selenide (Ag-As_2Se_3) Waveguides for Compact Nonlinear Optical Devices. *IEEE ThL3*, 2012.

[50] Bill P.-P. Kuo, John M. Fini, Lars Grüner-Nielsen, and Stojan Radic. Dispersion-stabilized highly-nonlinear fiber for wideband parametric mixer synthesis. *Optics Express*, 20(17), 2012.

[51] Magnus Karlsson. Four-wave mixing in fibers with randomly varying zero-dispersion wavelength. *J. Opt. Soc. Am. B*, 15(8), 1998.

[52] Mitra Farahmand and Martijn de Sterke. Parametric amplification in presence of dispersion fluctuations. *Optics Express*, 12(1), 2004.